

## **Water-Gas Shift Kinetics over Iron Oxide Catalysts at Membrane Reactor Conditions**

Reporting Period Start Date: 6/30/99  
Reporting Period End Date: 6/29/02

Final Report\*

Principal Author: Carl R. F. Lund

August 2, 2002

DOE Award No.: DE-FG2699-FT40590

Chemical Engineering Department  
University at Buffalo (SUNY-Buffalo)  
Buffalo, NY 14260-4200

\*The annual report for the period 6/30/01 to 6/29/02 is incorporated within

## **Disclaimer**

This report was prepared as an account of work sponsored by an agency of the United States Government. Neither the United States Government nor any agency thereof, nor any of their employees, makes any warranty, express or implied, or assumes any legal liability or responsibility for the accuracy, completeness, or usefulness of any information, apparatus, product, or process disclosed, or represents that its use would not infringe privately owned rights. Reference herein to any specific commercial product, process, or service by trade name, trademark, manufacturer, or otherwise does not necessarily constitute or imply its endorsement, recommendation, or favoring by the United States Government or any agency thereof. The views and opinions of authors expressed herein do not necessarily state or reflect those of the United States Government or any agency thereof.

## Abstract

The kinetics of water-gas shift were studied over ferrochrome catalysts under conditions with high carbon dioxide partial pressures, such as would be expected in a membrane reactor. The catalyst activity is inhibited by increasing carbon dioxide partial pressure. A microkinetic model of the reaction kinetics was developed. The model indicated that catalyst performance could be improved by decreasing the strength of surface oxygen bonds. Literature data indicated that adding either ceria or copper to the catalyst as a promoter might impart this desired effect. Ceria-promoted ferrochrome catalysts did not perform any better than unpromoted catalyst at the conditions tested, but copper-promoted ferrochrome catalysts did offer an improvement over the base ferrochrome material. A different class of water-gas shift catalyst, sulfided CoMo/Al<sub>2</sub>O<sub>3</sub> is not affected by carbon dioxide and may be a good alternative to the ferrochrome system, provided other constraints, notably the requisite sulfur level and maximum temperature, are not too limiting. A model was developed for an adiabatic, high-temperature water-gas shift membrane reactor. Simulation results indicate that an excess of steam in the feed (three moles of water per mole of CO) is beneficial even in a membrane reactor as it reduces the rate of adiabatic temperature rise. The simulations also indicate that much greater improvement can be attained by improving the catalyst as opposed to improving the membrane. Further, eliminating the inhibition by carbon dioxide will have a greater impact than will increasing the catalyst activity (assuming inhibition is still operative). Follow-up research into the use of sulfide catalysts with continued kinetic and reactor modeling is suggested.

<b>Table of Contents</b>	<b>Page</b>
Title Page .....	1
Disclaimer .....	2
Abstract .....	3
Table of Contents .....	4
List of Figures .....	5
List of Tables .....	6
Introduction .....	7
Executive Summary .....	8
Experimental .....	10
Results and Discussion .....	16
Conclusion .....	21
References .....	22
Bibliography .....	23
Tables .....	25
Figures .....	27

<b>List of Figures</b>	<b>Page</b>
Figure 1. Schematic representation of (a) a conventional WGS reactor system, and (b) a WGS membrane reactor. ....	27
Figure 2. Low (a) and high (b) magnification SEM images of the FeCr catalyst from which Cu-promoted catalysts were prepared. ....	28
Figure 3. Low (a) and high (b) magnification SEM images of the FeCr catalyst promoted with 1 wt.% Cu. ....	29
Figure 4. Low (a) and high (b) magnification SEM images of the FeCr catalyst promoted with 5 wt.% Cu. ....	30
Figure 5. With the overall reaction far from thermodynamic equilibrium (filled triangles), inhibition of WGS catalyst activity by CO <sub>2</sub> is evident in Bohlbro's data (filled circles) and is captured by the two-step microkinetic model (filled squares). The unfilled squares show the behavior of a hypothetical catalyst where the inhibition by CO <sub>2</sub> has been mathematically eliminated as described in the text. ....	31
Figure 6. Carbon monoxide conversion predicted by the six step microkinetic mode compared to that measured experimentally by Bohlbro. Bohlbro's data have been grouped into sets with a common temperature and pressure. ....	32
Figure 7. Comparison of the six step model predictions to experimentally measured CO conversions in a series of experiments at 653 K and 1 atm wherein Bohlbro varied the inlet CO <sub>2</sub> and N <sub>2</sub> partial pressures holding all other settings constant. ....	33
Figure 8. Simulated CO conversions for a set of "virtual" catalysts with one bond strength increased by 2% (1% in the case of HO*) from the values given in Table 2; the simulated experiments correspond to those in Figure 7. ....	34
Figure 9. Simulated CO conversions for a set of "virtual" catalysts with one bond strength decreased by 2% from the values given in Table 2; the simulated experiments correspond to those in Figure 7. ....	35
Figure 10. Simulated CO conversion as the O* bond strength is varied from the value in Table 2; conditions correspond to the experiment in Figure 7 with an inlet CO <sub>2</sub> /CO ratio of 2.0. ....	36
Figure 11. Carbon monoxide conversion predicted by the two step microkinetic model compared to that measured experimentally by Bohlbro. Bohlbro's data have been grouped into sets with a common temperature and pressure. ....	37
Figure 12. Effect of inlet steam to carbon monoxide ratio on the hydrogen yield and number of adiabatic stages. ....	38

Figure 13. Hydrogen yield as a function of catalyst volume for staged adiabatic membrane reactors with varying inlet steam to carbon monoxide ratios. ....	39
Figure 14. Variation in the percent of reaction equilibration and the percent of permeation equilibration along the length of an adiabatic staged membrane reactor. ....	40
Figure 15. Comparison of the simulated membrane reactor yield to idealized membrane reactors where either the membrane is perfect, the catalyst is perfect or the catalyst does not suffer from CO <sub>2</sub> inhibition. ....	41
Figure 16. Effect of Ce promoters on the activity of iron oxide WGS catalysts. ....	42
Figure 17. Effect of Cu promoter loading upon catalytic activity at membrane reactor conditions. ....	43
Figure 18. Effect of CO <sub>2</sub> upon the water-gas shift activity of sulfided CoMo/Al <sub>2</sub> O <sub>3</sub> . ....	44

#### **List of Tables**

**Page**

Table 1. BET Surface Areas of Fresh and Used Catalysts. ....	25
Table 2. Parameters for the Six-Step Microkinetic Model. ....	25
Table 3. Parameters for the Two-Step Microkinetic Model. ....	26

## Introduction

Water-gas shift, equation (1), is a well-studied and highly optimized commercial process that is practiced using conventional packed bed reactors. The engineering challenge in WGS derives from its reversibility and exothermicity. Elevated reaction temperatures are desirable because they correspond to higher rates and smaller volumes of catalyst, but reduced temperatures are required to reach greater equilibrium conversions. Current WGS practice, for example in ammonia synthesis plants, uses excess steam in the WGS feed. This has two beneficial effects upon conversion. It increases the equilibrium conversion due to the excess reactant and it also decreases the adiabatic temperature rise, again leading to increased equilibrium conversion. Addition of excess steam alone is not usually sufficient, however, and consequently the reaction is run in adiabatic stages with cooling between the stages. The first stage operates at a higher average temperature, using a promoted ferrochrome catalyst which has an operating range of ca. 600 to 750K [1]. The final stage operates at a lower average temperature using a CuZn-based catalyst which has a maximum operating temperature of ca. 530 to 560K [2]. Figure 1a presents a schematic representation of a conventional process.



It has been suggested that a membrane reactor might represent an alternative approach to efficient WGS following coal gasification. The gasification of coal produces a mixture of gases that includes H<sub>2</sub>O, CO, CO<sub>2</sub> and H<sub>2</sub>. These gases are generated at moderately high temperatures. If the coal is being gasified for the purpose of making transportation fuels that can substitute for gasoline, then following coal gasification the product gas will be fed to a Fischer-Tropsch process. Before doing so, WGS will likely be necessary to adjust the CO/H<sub>2</sub> ratio because the ratio exiting the gasifier will not normally be suitable for direct use in Fischer-Tropsch processing. The CO/H<sub>2</sub> ratio required for hydrocarbon synthesis varies between 1:1 and 1:3 depending on the desired hydrocarbon product. Alternatively, if the coal is being gasified for the purpose of making H<sub>2</sub> fuel, perhaps with sequestration of the co-produced CO<sub>2</sub>, then WGS will likely be used to convert as much as is practical of the CO into CO<sub>2</sub>.

In this context, a membrane reactor process offers some attractive features, particularly the ability to generate 100% pure H<sub>2</sub> while simultaneously producing a stream consisting predominantly of CO<sub>2</sub> that could be sequestered to mitigate global warming effects. A representative design for a membrane reactor process is shown schematically in Figure 1b. The reaction would likely take place adiabatically and at higher temperature and pressure. The higher pressure provides the driving force for permeation of the H<sub>2</sub> product through the Pd membrane. While the reactor would likely still be operated in stages to keep the temperature within the operational range of the catalyst, there is no need to use lower temperatures in the final stage because the in-situ separation will lead to a high H<sub>2</sub> yield even at higher temperatures. It would not be necessary to use an excess of steam in order to favor higher conversion, either, though it may still be useful with respect to lowering the adiabatic temperature rise and preventing carbon deposition. Instead, the reaction would proceed to high levels of conversion because one reactant (H<sub>2</sub> in the case shown in Figure 1b) is selectively removed from the reaction zone of the reactor. As a consequence, the overall CO conversion in the reactor would be limited only by the outlet partial pressure of the H<sub>2</sub> that had permeated through the membrane. That is, the reaction could

proceed to the point where the partial pressure (or more correctly the fugacity) of  $H_2$  was equal on the two sides of the membrane and the reaction side was simultaneously at WGS reaction equilibrium.

This project is focused upon an issue associated with the use of membrane reactors that is not always taken into consideration. Since WGS is such a well-studied process, it is often assumed that the catalysts used in present commercial processes will be equally effective when used in a membrane reactor like that shown in Figure 1. In fact, current high temperature WGS catalysts are quite effective when excess steam is present. However,  $CO_2$  is known to inhibit the reaction and lower the reaction rate over high temperature WGS catalysts. In a membrane reactor the concentration of  $CO_2$  will build to very high levels since the other product is being removed through the membrane. Hence, while current high temperature catalysts are quite effective and sufficiently active when used in traditional WGS processes, they may not be suitable for use in membrane reactor processes.

The project was undertaken with three broad objectives. The first objective was to study the kinetics of WGS over a ferrochrome catalyst at conditions characteristic of a membrane reactor, i.e. at high  $CO_2$  partial pressures. The results would then be used to develop a microkinetic model for WGS over these catalysts. The second broad objective was to develop a model for an adiabatic, high temperature water-gas shift membrane reactor like that shown in Figure 1b. This membrane reactor model would then be used to assess the performance of WGS catalysts, and to identify ways in which the catalytic performance might be improved. The third broad objective was to subsequently explore new catalyst formulations (either new classes of catalytic materials or promoters for the existing ferrochrome catalysts) that would lead to improved membrane reactor performance.

This report will demonstrate that the objectives of the original proposal were met, resulting in a successful project. More specifically, results are presented in the following topical areas: preliminary results from an investigation simulating selective removal of  $CO_2$  instead of selective removal of  $H_2$ , development of a microkinetic model for use in catalyst design, development of a microkinetic model for use in membrane reactor simulations, development of a model for an adiabatic, high temperature water-gas shift membrane reactor and its use to assess catalyst performance, microkinetically guided identification of catalyst promoters to improve membrane reactor performance of ferrochrome catalysts, and preliminary assessment of sulfur-tolerant water-gas shift catalysts for membrane reactor use.

## Executive Summary

The catalytic activity of conventional iron/chrome oxide high temperature water-gas shift catalysts is severely inhibited at high CO<sub>2</sub> partial pressures. If a membrane reactor is developed and used to drive water-gas shift to high conversions, it will likely function by selectively removing H<sub>2</sub> through the membrane. This will cause the CO<sub>2</sub> partial pressure to build even faster than it does in a conventional reactor, exacerbating this product inhibition phenomenon. Conventional water-gas shift processes utilize excess steam both to drive conversion and to reduce the rate of adiabatic temperature rise. In a membrane reactor excess steam would not be needed to push conversion, but it might still be desirable to control the rate of temperature rise. The objectives of this project were to assess the performance of conventional high temperature water-gas shift catalysts under membrane reactor conditions and then to identify or develop catalysts that will perform better under such conditions. These objectives were met, and the following specific conclusions reached.

*The kinetics of high temperature water-gas shift over a ferrochrome catalyst can be described accurately using a six step reduction/oxidation (redox) mechanism.* This mechanism provides useful insight in the design of new, promoted catalysts. A microkinetic model, based upon this mechanism, indicates that catalyst activity can be raised by decreasing the bond strength of surface oxygen atoms. The open literature suggests that addition of either Ce or Cu as a promoter might cause such a decrease in surface oxygen bond strength.

*The addition of Ce to a ferrochrome catalyst as a promoter does not measurably improve its performance under high-temperature water-gas shift at membrane reactor conditions.*

*The addition of Cu to a ferrochrome catalyst as a promoter improves its performance under high-temperature water-gas shift at membrane reactor conditions.* There is an optimum in the amount of added Cu at approximately 10 wt%; additional Cu has little effect upon performance.

*The kinetics of high temperature water-gas shift over a ferrochrome catalyst also can be described accurately using a two step redox mechanism.* This mechanism is particularly useful in performing membrane reactor simulations because it is mathematically more tractable. It is only slightly less accurate than the six step mechanism, but it does accurately capture the critical inhibition effect of CO<sub>2</sub>.

*While excess steam is not required to push conversion in a membrane reactor, it is still desirable for controlling the rate of temperature rise in an adiabatic membrane reactor.* This conclusion is based upon the simulation of a membrane reactor using the microkinetic model developed as a part of this project with reasonable membrane parameters (for a Pd membrane). The simulation indicates an inlet feed composition of 3 H<sub>2</sub>O per CO is optimum; it leads to only two adiabatic stages and achieves its ultimate conversion in the smallest catalyst volume.

*The limiting factor in a high temperature water-gas shift membrane (Pd) reactor studied here is the rate of reaction and not the rate of permeation through the membrane.* This conclusion is also based upon simulation results. The simulations show that replacing the Pd membrane with a perfect membrane has a much smaller effect upon membrane reactor performance than does replacing the catalyst with a perfect catalyst. This conclusion suggests that development of better catalysts should have a greater priority than development of better membranes.

*Removing the inhibitory effect of CO<sub>2</sub> leads to much greater gains in H<sub>2</sub> yield than would finding a perfect membrane material.* This conclusion again is based upon membrane reactor

simulation. It suggests that within the catalyst design arena, it is more important to focus upon eliminating inhibition by  $\text{CO}_2$  than to focus upon increasing catalyst activity.

*Catalysts based upon sulfided  $\text{Mo}/\text{Al}_2\text{O}_3$  are not inhibited by  $\text{CO}_2$  in the way that ferrochrome catalysts are inhibited.* These materials may be good candidates for use in a medium-temperature membrane reactor, but further study will be necessary to determine whether their required sulfur levels can be tolerated by the membrane.

## Experimental

Catalyst Preparation and Characterization. Several different catalysts were used experimentally. Unpromoted iron oxide came from three sources. The first was purified grade iron oxide powder obtained from Fisher Scientific. A second was precipitated from an aqueous mixture of ferrous and ferric ammonium sulfates using ammonium hydroxide as described in the literature [3]. The third source was simple calcination of iron nitrate. Cerium promoted iron oxide was prepared by mixing cerium nitrate and the iron oxide powder in ethanol and then evaporating the solvent. A doubly promoted (Ce and Cr) catalyst was prepared by precipitation from an acidified aqueous solution of ferrous sulfate, ferric sulfate, chromium sulfate and cerium sulfate using ammonium hydroxide. A Cr promoted catalyst was prepared by precipitation from an aqueous solution of ferric and chromium sulfate. Finally, a series of Cu promoted catalysts was prepared by mixing the FeCr catalyst and copper nitrate in ethanol and evaporating the solvent.

The prepared catalysts were examined using scanning electron microscopy, and selected results are presented in Figures 2 through 4. The micrographs indicate that the copper promoted catalysts were structurally similar to the unpromoted material. There is no evidence of a separate copper-containing phase in the samples. This indicates that the copper was well distributed over the surface of the iron-chrome oxide. Unpromoted iron oxide catalysts are known to sinter during use in WGS. Therefore, the BET surface area of representative catalysts was measured after preparation and again after use in the reactor. The results are presented in Table 1.

Experimental Catalyst Activity Measurements. A new reactor system was fabricated and used to measure the kinetics of the WGS reaction. CO (Cryogenic Supply, CP grade), CO<sub>2</sub> (Cryogenic, Bone Dry Grade), H<sub>2</sub> (Cryogenic, Pre-purified Grade) and Ar (Cryogenic, High Purity Grade) were fed from cylinders. Each feed line running between the feed cylinder and an Omega FMA-A2402 mass flow controller included a pressure relief valve. The gases exiting the flow controllers were mixed in a common manifold which flowed to a packed bed of 100 mesh glass beads (Alltech) housed in a tube furnace. The temperature in this tube furnace was set using a variac power controller and was monitored using an Omega 115KC temperature readout. Water was also fed to the packed bed from an ISCO Series D syringe pump and controller. The lines leaving the tube furnace up to the point of the water condenser (see below) were all heat traced to prevent the condensation of water. From the packed bed where the water was vaporized, the gases flowed to the first inlet port of a sampling valve on an SRI 8610 gas chromatograph. A gc column packed with 80-100 mesh Porapak QS (Alltech) was used to separate the gases, which were detected using a thermal conductivity detector. CO and CO<sub>2</sub> were then methanized and also detected using a flame ionization detector. A personal computer running PeakSimple II (SRI) was used for data collection and analysis. From the outlet of the first sampling port on the gc, the gases flowed to two three-way switching valves that could be used either to direct the gases to the reactor or to bypass the reactor.

The reactor consisted of a vertically oriented stainless steel tube with a 0.25 in diameter and a 14 in length. A sheathed thermocouple entered the tube coaxially from the top and extended into the catalyst bed, and a second one entered from the bottom, extending into the reactor tube below the catalyst bed. These thermocouples were used to monitor the bed and reactor temperature. The reactor was positioned within a split tube furnace (Lindberg type 54231). The thermocouple built into the furnace was used to control the temperature via an Omega CN9000A temperature controller. The catalyst bed rested upon glass wool, centered within the furnace.

From the reactor the gases flowed back to the other side of the bypass valve set and continued to the second inlet port of the gas chromatograph sampling valve. After leaving the gas chromatograph, the gases flowed to a condenser where water was removed. This was followed by a backpressure regulator that was used to set the pressure in the reactor. The pressure was reduced to atmospheric following the backpressure regulator, whereupon the flow rate could be checked with a bubble flow meter or the gas could be vented to a hood.

Typically, ca. 0.5 g of catalyst were packed in the reactor and the reactor temperature, pressure and feed composition were set to desired levels. The system was allowed to attain steady state. After steady state had been attained, the inlet and outlet composition was measured using the gas chromatograph. At least three sets of inlet and outlet analyses were used to ensure the system had indeed reached steady state. The inlet composition was determined from the full gas chromatographic analysis of the inlet gas stream. The CO conversion,  $x_{CO}$ , was calculated using equation (2) and the inlet and outlet ratios of CO<sub>2</sub> to CO, as measured gas chromatographically.

$$x_{CO} = \frac{\left(\frac{CO_2}{CO}\right)_{out} - \left(\frac{CO_2}{CO}\right)_{in}}{1 + \left(\frac{CO_2}{CO}\right)_{out}} \quad (2)$$

Microkinetic Modeling for Catalyst Design. Equations (3) through (8) were selected to describe the conversion of CO. These equations postulate that paired sites are responsible for the catalytic activity. CO is assumed to adsorb as a bidentate carbonate species on a fully oxidized, paired site, equation (3), followed by rearrangement to a unidentate carbonate occupying a partially reduced paired site, equation (4). CO<sub>2</sub> then desorbs leaving a partially reduced paired site, equation (5). Water is presumed to adsorb initially on the reduced portion of the resultant paired site, equation (6), and then to dissociate generating two hydroxyl groups, equation (7). Associative desorption of H<sub>2</sub>, equation (8) then regenerates a fully oxidized paired site and completes the catalytic cycle.

The mechanism of equations (3) through (8) was fit to Bohlbro's data using an approach similar to that described by Dumesic et al. [4]. An expression for the net rate of each mechanistic step was written using simple transition state theory. Thus, for example, the expression for the net rate of reaction (6) is given by equation (9) where  $k_6^0$  represents the pre-exponential factor of the forward rate coefficient,  $E_6$  represents the activation energy,  $\Delta S_6$  represents the standard entropy change associated with reaction (6) and  $\Delta H_6$  represents the standard enthalpy change. The standard entropy and enthalpy changes of the reaction steps were then expressed in terms of the standard entropies and enthalpies of formation of the participant species. Thus, the standard entropy and enthalpy changes for reaction (6) were expressed using equations (10) and (11).





$$r_{6,net} = k_6^0 \exp\left(\frac{-E_6}{RT}\right) \left[ P_{\text{H}_2\text{O}} \theta_* - \frac{\theta_{\text{H}_2\text{O}^*}}{\exp\left(\frac{\Delta S_6}{R}\right) \exp\left(\frac{-\Delta H_6}{RT}\right)} \right] \quad (9)$$

$$\Delta S_6 = S_{\text{H}_2\text{O}^*}^0 - S_*^0 - S_{\text{H}_2\text{O}}^0 \quad (10)$$

$$\Delta H_6 = \Delta_f H_{\text{H}_2\text{O}^*}^0 - \Delta_f H_*^0 - \Delta_f H_{\text{H}_2\text{O}}^0 \quad (11)$$

The entropies of formation,  $S_i^0$ , and enthalpies of formation,  $\Delta_f H_i^0$ , for the gas phase species,  $i$ , are known functions of temperature. Here, these quantities were represented using the Shomate equation, with appropriate parameters obtained from the NIST Chemistry Webbook [5]. The entropies of formation for the surface species were estimated starting with the gas phase value at the average experimental temperature, 688 K, and then subtracting the corresponding ideal gas translational entropy. The resulting entropies of formation of the surface species were held constant. Similarly, the enthalpies of formation for the surface species were estimated starting with the gas phase value at 688 K and then subtracting the net bond strength between that species and the surface,  $-\Delta H_{i_{\text{gas}} \rightarrow i_{\text{surface}}}^0$ . The latter quantities constituted one set of adjustable parameters that were used to fit the microkinetic model to the experimental data. The pre-exponential factors,  $k_j^0$ , for each of the reactions,  $j$ , were estimated on the basis of simple transition state theory or collision theory and then held constant, as well. Finally, the activation energies,  $E_j$ , for each of the reactions,  $j$ , constituted a second group of adjustable parameters that were used to fit the microkinetic model to the experimental data.

To fit the microkinetic model to the experimental data, material balance equations were written for every species except the vacant site, assuming the reactor to have operated in isothermal, isobaric plug flow. This resulted in a model that consisted of a set of coupled algebraic and ordinary differential equations to which was added the requirement that the sum of the fractional coverages over all the surface species, including the vacant site, must equal one. For a given set of adjustable parameters (the set of surface bond strengths and the activation energies) this model could be solved to predict the CO conversion. This was repeated, varying the values of the adjustable parameters, until the sum of the squares of the differences between the predicted CO conversions and the experimentally measured CO conversions was minimized. This process was automated using Athena Visual Workbench [6].

Microkinetic Modeling for Membrane Reactor Simulations. The microkinetic model described above can be difficult to use in a membrane reactor simulation because the set of coupled differential and algebraic equations don't converge easily in some situations. To reduce the difficulty associated with membrane reactor modeling, a second microkinetic model was developed. Specifically, the kinetics were described in terms of the simple redox mechanism presented in equations (12) and (13). The entropy of formation for the surface oxygen was estimated starting with its gas phase value at the average experimental temperature, 688 K, and then subtracting its ideal gas translational entropy. The resulting entropy of formation was held

constant during the fitting process. Similarly, the enthalpy of formation for the surface oxygen was estimated starting with its gas phase value at 688 K and then subtracting the net strength of the bond or bonds holding it to the surface,  $-\Delta H_{O_{gas} \rightarrow O^*}^0$ . The pre-exponential factors,  $k_j^0$ , for each of the reactions,  $j$ , were estimated on the basis of simple transition state theory or collision theory and then held constant during the fitting process, as well. This left the two activation energies,  $E_{12}$  and  $E_{13}$ , along with  $-\Delta H_{O_{gas} \rightarrow O^*}^0$  as the three adjustable parameters that were used to fit the microkinetic model to the experimental data.



Membrane Reactor Modeling. The schematic diagram of Figure 1b formed the basis for simulation of membrane reactor performance. It was assumed that the catalyst would be packed inside a cylindrical membrane tube, and that the reactor would operate adiabatically, at constant pressure, at steady state, and in plug flow. The microkinetic model just described was used to represent the reaction kinetics. Ferrochrome high temperature shift catalysts have an operational temperature range of ca. 600 to 750K [1], so it was assumed that the feed would enter at 600K, and that when the temperature reached 750K the process stream would be cooled back to 600K and then fed to the next adiabatic stage of the membrane reactor. (The figure only shows a single stage.) In other words, no attempt was made to optimize the temperature profile. The diameter of the membrane tube was assumed to be 0.25 in and the Pd thickness to be 10  $\mu\text{m}$ . It was assumed that the pressure inside the membrane tube (where reaction takes place) was 1000 psia and that the pressure outside the membrane tube was 1 atm (14.7 psia). This pressure differential was assumed to provide the driving force for hydrogen permeation through the membrane, so no inert sweep gas would be needed on the receiving, or permeate, side of the membrane. The permeability of hydrogen through the Pd membrane was assumed to follow Sievert's law using the temperature dependent permeance reported by Shu et al. [7]. With these assumptions, the membrane reactor model consisted of a set of seven coupled algebraic and ordinary differential equations given as equations (14) through (20). In these equations  $\dot{n}_i$  represents the molar flow rate of species  $i$ ,  $m$  denotes the catalyst mass,  $A_m$  represents the membrane area per mass of catalyst,  $P_0$  is the pre-exponential term of the permeance,  $E_P$  is the activation energy of the permeance,  $P_P$  is the permeate side pressure (1 atm), and  $\hat{C}_{p-i}$  is the molar specific heat capacity of species  $i$  (calculated using the Shomate equation and NIST Chemistry Webbook data [5]). The inlet molar flow rates were used as the initial conditions for equations (14) through (17), and 600K was used as the initial condition for equation (18). The model equations were solved using Athena Visual Workbench [6].

$$\frac{d\dot{n}_{\text{CO}}}{dm} = -r_{12,net} \quad (14)$$

$$\frac{d\dot{n}_{\text{H}_2\text{O}}}{dm} = -r_{13,net} \quad (15)$$

$$\frac{d\dot{n}_{CO_2}}{dm} = r_{12,net} \quad (16)$$

$$\frac{d\dot{n}_{H_2}}{dm} = r_{13,net} - A_m P_0 \exp\left(\frac{-E_p}{RT}\right) \left(\sqrt{P_{H_2}} - \sqrt{P_p}\right) \quad (17)$$

$$\frac{dT}{dm} = \frac{-r_{12,net} \Delta H_{12} - r_{13,net} \Delta H_{13}}{\dot{n}_{CO} \hat{C}_{p-CO} + \dot{n}_{H_2O} \hat{C}_{p-H_2O} + \dot{n}_{CO_2} \hat{C}_{p-CO_2} + \dot{n}_{H_2} \hat{C}_{p-H_2}} \quad (18)$$

$$r_{12,net} = r_{13,net} \quad (19)$$

$$1 = \theta_{O*} + \theta_* \quad (20)$$

In order to assess the performance of the membrane reactor, comparison was made to three idealized situations. The first corresponded to a perfect membrane. In this case, permeation was assumed to occur instantaneously. As a consequence, the partial pressure of H<sub>2</sub> on the reaction side of the membrane was set equal to the permeate side pressure of 1 atm, and equation (17) was removed from the set of model equations. The second idealized situation corresponded to a perfect catalyst. In this case, model consisted of only equation (21). The other molar flow rates and the temperature were calculated by assuming that the reaction was always at thermodynamic equilibrium (with a corresponding adiabatic temperature rise).

$$\frac{d\dot{n}_{H_2}}{dm} = -A_m P_0 \exp\left(\frac{-E_p}{RT}\right) \left(\sqrt{P_{H_2}} - \sqrt{P_p}\right) \quad (21)$$

The third idealized situation was related to the known inhibition of ferrochrome high temperature shift catalysts by CO<sub>2</sub>. Figure 5 plots a series of kinetic runs from Bohlbro's data set [1] wherein the inlet partial pressures of CO and H<sub>2</sub>O were held constant along with the total flow rate and temperature. The partial pressure of CO<sub>2</sub> and that of N<sub>2</sub> make-up gas were the only parameters varied. The figure shows that while the reaction was far from thermodynamic equilibrium the experimental CO conversion decreased from over 20% in the absence of CO<sub>2</sub> to less than 5% when CO<sub>2</sub> was added. This is due to inhibition by CO<sub>2</sub>; Bohlbro found the order of the reaction with respect to CO<sub>2</sub> to be ca. -0.6. The figure shows that the microkinetic model captures this inhibition effect, as well. In the third idealized situation, this inhibition by CO<sub>2</sub> was removed from the kinetic behavior. To do this, the rate expressions corresponding to equations (12) and (13) were evaluated at prevailing conditions, except that the partial pressure of CO<sub>2</sub> was set to an arbitrary low partial pressure. This partial pressure (0.0288 atm) was selected so that the predicted conversion at CO<sub>2</sub>/CO = 0 in Figure 5 would match the experimental conversion. In doing this, the rate expression would not display the proper limiting behavior as the conversion approaches equilibrium, so the resulting rate was multiplied by a term that ensures proper limiting behavior at thermodynamic equilibrium. This is shown in equation (22), where  $K$  denotes the temperature dependent equilibrium constant for the overall water-gas shift reaction and  $r_{j,NI}$  represents the rate in the absence of CO<sub>2</sub> inhibition. Figure 5 shows that the use of this

rate expression leads to a predicted conversion that matches the experimental results at low CO<sub>2</sub>/CO, but as the CO<sub>2</sub>/CO ratio is increased, the conversion holds essentially constant, i. e. inhibition by CO<sub>2</sub> is eliminated.

$$r_{j,NI} = \left( 1 - \frac{P_{H_2} P_{CO_2}}{K P_{CO} P_{H_2O}} \right)^3 r_{j,net} \Big|_{P_{CO_2}=0.0288 \text{ atm}} \quad (22)$$

## Results and Discussion

Preliminary Results from Reactor Studies. While a membrane reactor will most likely remove H<sub>2</sub> selectively, reaction/separation processes for water-gas shift have been proposed wherein CO<sub>2</sub> is selectively removed. Therefore experiments were also performed where varying amounts of H<sub>2</sub> were added to a stoichiometric feed. The feed contained about 11% CO and 12% H<sub>2</sub>O at ca. 2.5 atm and 8.5 WHSV. Experiments were conducted at 673 and 733 K. When the hydrogen partial pressure was increased to ca. 0.3 atm, new products were detected in the reactor outlet. It appears that as the hydrogen partial pressure is increased, the catalyst is reduced from iron oxide to metallic iron. With unreacted CO still present, this most likely led to methanation and other Fischer-Tropsch type chemistry.

This suggests that a conventional iron oxide-based catalyst also will not perform well in a reaction/separation process that selectively removes CO<sub>2</sub>. However, the experiments leading to this conclusion involved nearly equimolar reactants. It will be seen subsequently, that an excess of steam, ca. 3 H<sub>2</sub>O per CO, is preferable, even in a membrane reactor because the excess steam reduces the rate of adiabatic temperature rise. The reduction of the catalyst and onset of Fischer-Tropsch chemistry observed experimentally might not occur if excess steam was used. This topic was not pursued nonetheless, because the PI was not aware of any membrane or other reactive separation schemes that could operate at temperatures where ferrochrome catalysts are active. For example, facilitated transport membranes have a maximum temperature well below 600K. The remainder of the project was focused upon systems where H<sub>2</sub> is selectively removed since membrane materials are available for this application and they can operate at temperatures where ferrochrome shift catalysts are active.

Microkinetic Model for Catalyst Design. Bohlbro reported an extensive study of the kinetics of high temperature water-gas shift over iron-chrome catalysts [1]. In that work, the kinetics were modeled using power-law rate expressions. In the present study, Bohlbro's data were used initially to develop a microkinetic model for water-gas shift over an iron-chrome catalyst. Different mechanisms have been proposed over the years to account for high temperature shift catalysis [8-16]. The present purpose was not to compare the adequacy of different mechanistic models. A relatively simple redox mechanism involving carbonate and hydroxyl surface species was formulated as described above and used. No claim is made that this mechanism prevails under reaction conditions. It will simply be shown here that this mechanism fits the experimental data well and that it can be used to make predictions for improving catalyst performance at membrane reactor conditions. Since, do date, those predictions proved accurate and led to improved catalyst performance, the microkinetic model has served its purpose (even if the mechanism is not correct); had the model not worked as well as it did, other mechanistic descriptions would have been considered.

The optimized values of the adjustable parameters of the six-step redox mechanism, along with the fixed quantities are presented in Table 2. These parameters are reasonable. The fitted value of  $E_4$  is  $0 \text{ kJ mol}^{-1}$ . This suggests that  $\text{CO}_2$  may actually desorb directly from the bidentate surface carbonate. Figure 6 plots the CO conversions predicted by the model against those measured experimentally. The figure shows that the fit is generally good, taking the experimental uncertainty into consideration. Indeed, in the original work Bohlbro grouped experimental runs according to temperature, pressure, etc. and used different sets of power-law parameters for different groups of results; here all the data were fit using a single set of microkinetic parameters.

Figure 7 shows Bohlbro's experimental results and microkinetic model predictions for the series of experiments wherein the inlet partial pressure of  $\text{CO}_2$  was increased while holding all other settings constant (the same set of experiments as is shown in Figure 5). It has already been noted that in a membrane reactor, the  $\text{CO}_2$  partial pressure is expected to rise to high values as the reaction proceeds due to the removal of  $\text{H}_2$ . Figure 7 shows that as the partial pressure of  $\text{CO}_2$  increases, the catalytic activity, reflected in the CO conversion, falls significantly. The effect of this catalyst inhibition by  $\text{CO}_2$  upon the operation of a membrane reactor can be seen by considering a membrane reactor operating at 733 K and 1000 psia (6890 kPa) with a stoichiometric feed and with 95% recovery of  $\text{H}_2$  through the membrane. The present microkinetic model predicts that the rate of water-gas shift will have decreased by three orders of magnitude by the time 90% of the CO has been converted.

This raises the question whether catalyst performance could be improved, somehow. To address this question, "virtual" catalysts were tested using the microkinetic model. To start, each "virtual" catalyst was created by increasing or decreasing the surface bond strength of one species by 2%. The performance of the resulting virtual catalyst was simulated at the same conditions as those of Figure 7. The results are plotted in Figures 8 and 9 where it can be seen that most bond strengths do not strongly affect performance. Decreasing the  $\text{O}^*$  bond strength is the only change that is predicted to improve catalyst performance. Intuitively, it had been expected that weakening the surface carbonate bond strength would lessen the inhibitory effect of  $\text{CO}_2$ , but the results do not show this to be so.

A second set of "virtual" catalysts was created by varying the  $\text{O}^*$  bond strength. The performance of this series of "virtual" catalysts was simulated at conditions corresponding to the experiment in Figure 7 with an inlet  $\text{CO}_2/\text{CO}$  ratio of 2.0. The results are shown in Figure 10. It can be seen that the model predicts a 4.4-fold increase in CO conversion as the  $\text{O}^*$  bond strength is weakened by 5%, at which point the effect saturates. Thus, the model suggests that one might improve the membrane reactor performance of high temperature iron-chrome shift catalysts by modifying them in ways that will decrease the surface oxygen bond strength.

Papers by Hu et al. [17] and Kappen et al. [18] provided a starting point for attempting to synthesize real catalysts with weaker surface oxygen bond strengths. These papers report that the addition of Ce or Cu as a promoter to an iron-chrome shift catalyst changes their behavior during temperature programmed reduction (TPR). Specifically, the addition of either of these promoters leads to a shift in the TPR peak to lower temperatures. While there could be other causes, this lowering of the peak TPR temperature may be indicative of a weaker surface oxygen bond. Experimental studies of the effects of adding Ce and Cu are discussed below.

Microkinetic Model for Membrane Reactor Simulation. Figure 11 plots the CO conversions predicted by the two-step microkinetic model against those measured experimentally. The figure shows that the fit is generally good, taking the experimental

uncertainty into consideration. Statistically the fit is not quite as good as with the six step model, but here there are only three adjustable parameters. The optimized values of the adjustable parameters, along with the microkinetic modeling parameters that were held fixed, are presented in Table 3, and their values are seen to be reasonable. As with the six-step model, it is not claimed that the simple two step mechanistic model truly represents the molecular phenomena involved in the reaction; all that is desired is a kinetic model that accurately predicts the rate of reaction. Figures 5 and 11 show that this has been achieved, and most importantly, the microkinetic model predicts the inhibitory effect of CO<sub>2</sub> as can be seen in Figure 5.

Adiabatic, High Temperature Water-Gas Shift Membrane Reactor Assessment. The membrane reactor model used here is relatively simple. Nonetheless, similar models have been used to simulate an isothermal Pd membrane reactor [7, 19], finding very good agreement between the model's predictions and actual measurements from a laboratory membrane reactor. Here the reactor is assumed to operate adiabatically, adding one additional equation to the model. Given the demonstrated accuracy of the isothermal model, it is believed that the present simulations offer a very reasonable first-order approximation of adiabatic membrane reactor performance.

In a membrane reactor, the use of excess steam can have at least three effects: it can help prevent carbon deposition at the inlet to the reactor, it will reduce the adiabatic temperature rise, and it may reduce the reaction rate (Bohler's power law models show the rate to be approximately 0.9 order in CO and ca. 0.25 order in H<sub>2</sub>O). As already noted, excess steam leads to a greater equilibrium conversion in a conventional reactor, but that is not needed in a membrane reactor. To assess the effect of excess steam upon membrane reactor performance, four adiabatic membrane reactor simulations are compared in Figures 12 and 13. Figure 12 plots the final yield of H<sub>2</sub> (the moles of H<sub>2</sub> recovered through the membrane relative to the moles of H<sub>2</sub> that would be produced at 100% conversion of the limiting reagent) as a function of the number of adiabatic stages. In constructing this figure, additional stages were added until, in the final stage, the outlet temperature no longer reached 750K. The figure shows that for the conditions of the simulation, a H<sub>2</sub>O:CO feed ratio of 3 is optimum with respect to the number of adiabatic stages. Figure 13 shows the H<sub>2</sub> yield as a function of the cumulative mass of catalyst (equivalent to reactor size). It can be seen that again a H<sub>2</sub>O:CO feed ratio of 3 is optimum, reaching its ultimate final conversion with the least amount of catalyst. Clearly, the role of excess steam in reducing the adiabatic temperature rise overshadows any negative effect upon the reaction kinetics. Hence, in all remaining simulations in the present investigation, the inlet H<sub>2</sub>O:CO ratio was set equal to 3.

When seeking to develop a better high temperature water-gas shift membrane reactor, it is useful to be able to identify the rate-limiting process at any point within the reactor. Specifically, it is useful to know whether the rate of the chemical reaction or the rate of permeation through the membrane is rate-determining. In the present work, two approaches to making such an assessment have been employed. The first attempts to quantify the extent to which the reaction and permeation processes are locally equilibrated. To do so, consider an adiabatic membrane reactor like that described previously and shown schematically in Figure 1b. One can define a local percent of reaction equilibration,  $P_{RE}$ , as given in equation (23). If the local composition corresponds to thermodynamic equilibrium,  $P_{RE}$  will equal 100%. If no reaction has taken place,  $P_{RE}$  will equal 0%. For any single adiabatic stage,  $P_{RE}$  will always lie between these two extremes. Furthermore, since the reaction is exothermic and there is cooling between stages, there will always be a decrease in  $P_{RE}$  in passing from the outlet of one stage to the inlet of the

next, but it will never fall below 0%. Hence,  $P_{RE}$  represents a useful metric for assessing the local degree of reaction equilibration at any point in the multi-stage membrane reactor train.

$$P_{RE} = 100\% \left( \frac{P_{H_2} P_{CO_2}}{K P_{CO} P_{H_2O}} \right) \quad (23)$$

Considering the permeation process, it is equilibrated when the local  $H_2$  partial pressure (in the reaction zone) is equal to the permeate side pressure,  $P_P$ . At the opposite extreme, if no permeation had taken place, then the local partial pressure of  $H_2$  would be determined by the inlet  $H_2$  partial pressure,  $P_{H_2}^0$ , the inlet CO partial pressure,  $P_{CO}^0$ , and the CO conversion,  $x_{CO}$ . Using these two points of reference, a local percent of permeation equilibration,  $P_{PE}$ , can be defined as in equation (24). Examination of equation (24) shows that  $P_{PE}$  will equal 100% whenever the partial pressure of  $H_2$  is equilibrated across the membrane; it will equal 0% if no permeation has taken place. However, it should be noted that it is possible for  $P_{PE}$  to assume a negative value. This can happen near the inlet to the reactor where the conversion of CO is low, and consequently the  $H_2$  partial pressure has not yet built up to equal the permeate side pressure. At such a location,  $H_2$  may actually permeate from the permeate side of the membrane to the reaction side, and if this happens,  $P_{PE}$  will have a negative value. However, once the partial pressure of  $H_2$  has reached the permeate side pressure,  $P_{PE}$  will vary between 0% and 100%, and it will be unaffected by cooling between stages, so it is a useful metric for assessing the local degree of permeation equilibration at any point in a multi-stage membrane reactor train.

$$P_{PE} = 100\% \left( 1 - \frac{P_{H_2} - P_P}{P_{H_2}^0 + x_{CO} P_{CO}^0 - P_P} \right) \quad (24)$$

As already noted, an inlet  $H_2O:CO$  ratio of 3 leads to a membrane reactor that requires only two adiabatic stages (Figure 12) and that reaches equilibrium with the least amount of catalyst (Figure 13). The variation in the percent of reaction equilibration and the percent of permeation equilibration along the length of this reactor are plotted in Figure 14, which also reproduces the  $H_2$  yield results. Near the inlet to the reactor, the percentage of permeation equilibration is indeed negative as just described, but these data are not plotted in Figure 14. The most striking observation from Figure 14 is that the permeation process is far closer to being equilibrated than the reaction process almost everywhere within the reactor. More specifically, the percent permeation equilibration becomes greater than 90% at a catalyst mass of only 875 g while the percent reaction equilibrium has only reached 10% at a catalyst mass of ca. 4500 g.

This result may be surprising at first. It is often assumed that the rate of permeation through dense membranes like Pd is too slow for practical applications. The membrane thickness used here in the simulations is within the range of experimentally studied membranes, however. The conclusion that the reaction rate is the limiting process is also drawn upon examination of Figure 15. That figure shows that if the membrane in the reactor model is made perfect (instantaneous transport of the hydrogen through it) there is only a marginal gain in the hydrogen yield from the reactor. On the other hand, if the catalyst in the reactor model is made perfect (instantaneous equilibration of the reaction) there is a tremendous gain in hydrogen yield. For example, at a catalyst mass of ca 1000 g, the membrane reactor model predicts approximately

50% hydrogen yield with either a perfect membrane or a more realistic membrane. At the same catalyst mass the membrane reactor model predicts over 90% hydrogen yield for a realistic membrane with a perfect catalyst.

These results suggest that the most dramatic improvement in high temperature, adiabatic water-gas shift membrane reactor performance will be realized by finding improved catalysts, not by finding improved membranes. This can be seen in Figure 15 for the third idealized case; that where inhibition by CO<sub>2</sub> is removed. Simply eliminating the inhibition by CO<sub>2</sub> without changing the catalyst activity or anything associated with the membrane gives 90% hydrogen yield at a catalyst mass of ca. 1000g; inhibition by CO<sub>2</sub> lowers the yield from 90% to ~50%. Putting it another way, the simulations predict that for a 90% hydrogen yield, finding a perfect membrane would reduce reactor size by 12% whereas eliminating the inhibiting effect of CO<sub>2</sub> would reduce reactor size by 76%. Ferrochrome high-temperature water-gas shift catalysts have been used for a long time, and they have been studied extensively. As a consequence, it would not be a trivial task either to improve this catalyst or find a more suitable one. Nonetheless, the present results indicate that catalyst improvement will have a much greater impact upon membrane reactor performance than will membrane improvements.

More generally, the approach utilized here may be broadly applicable to the assessment of membrane reactors in so-called “equilibrium shifting” situations. Through membrane reactor modeling and simulation, one can compare the system of interest to idealized cases where either the catalyst is perfect or the membrane is perfect. Such a comparison may then suggest that development efforts should be focused either upon the membrane or upon the catalyst.

Promoters for Ferrochrome Catalysts. It is generally accepted that the role of chromia in a ferrochrome high temperature water-gas shift catalyst is to add structural stability. The experimental work in the present investigation was consistent with this interpretation. Specifically, it was observed that back-to-back runs using an unpromoted iron oxide catalyst (irrespective of preparation method) showed decreasing activity with time on stream. The BET data in Table 1 show that the unpromoted iron oxide underwent significant loss of surface area during its use. When Cr was added to the iron oxide catalyst, it did not give any indication of deactivation with use, and the BET data show that the surface area did not change appreciably. Thus, the Cr-promoted iron oxide catalyst was adapted as the base material for further study.

Hu et al. [17] reported that Ce-promotion improved an FeCr WGS catalyst. Among the results presented was a temperature-programmed reduction profile where the maximum reduction rate shifted to lower temperature with the promoted catalyst. The modeling work already described suggests that if this temperature shift is indicative of a weaker oxygen bond strength, then the Ce-promoted FeCr catalyst should be less susceptible to inhibition by CO<sub>2</sub>. Therefore, catalyst was synthesized following the procedure described by those authors, and it was tested in a series of experiments where the inlet CO<sub>2</sub> concentration was varied at fixed CO and H<sub>2</sub>O inlet concentrations. Additionally, two other catalysts were prepared with Ce promoter, but without the Cr.

Figure 16 shows the results for ceria-promoted catalysts with and without an additional Cr promoter, and compares them to an unpromoted iron oxide catalyst. There is no measurable difference in the susceptibility to inhibition by CO<sub>2</sub> for these catalysts. This result was disappointing, as the Ce promotion had no effect. It is suspected that the shift in the temperature-programmed reduction curves reported for Ce-promoted catalysts may be caused by the onset of CeO<sub>2</sub> reduction and thus may have no significance to the iron-oxygen surface bond strength.

Kappen et al. [18] reported the same kind of change in the temperature programmed reduction profile when an FeCr WGS catalyst was promoted with Cu. They noted that this could be an effect of differences in heating rate, preparation, or an effect of the presence of the copper promoter atoms. As with Ce, a series of catalysts was prepared for testing the effect of Cu promotion upon the inhibition by CO<sub>2</sub>. TPR experiments using these catalysts did show a small shift in the peak reduction temperature. The results from reactor studies are shown in Figure 17, where it can be seen that addition of Cu up to ca. 10 wt.% does indeed improve CO conversion in the presence of CO<sub>2</sub>.

Preliminary Assessment of Sulfur-Tolerant Catalysts. A microkinetic model for water-gas shift over sulfided Mo/Al<sub>2</sub>O<sub>3</sub> and sulfided CoMo/Al<sub>2</sub>O<sub>3</sub> was developed a few years ago [20, 21]. Since the mechanism of the reaction on these catalysts is believed to be very different from that on iron oxide catalysts, it seemed quite possible that the rate would not be inhibited by CO<sub>2</sub>. This was tested by simulation using the available microkinetic model for sulfided CoMo/Al<sub>2</sub>O<sub>3</sub>. Figure 18 shows the result of a series of simulations of a conventional reactor operating at 14.6 atm. and 548 K with a feed that contains varying amounts of CO<sub>2</sub>. There is very little inhibition of the rate as CO<sub>2</sub> is added to the feed; the conversion drops only 8% upon changing from a CO<sub>2</sub>/CO ratio of 0 to a ratio of 4. This is a promising lead that should be followed up.

There are also a few caveats that should be mentioned. First, these catalysts must have a sulfur source in order to maintain their activity. It appears that there are dense membrane materials that may function in the presence of low levels of H<sub>2</sub>S. For example, at a recent UCR contractors' meeting, Way [22] reported on one such material that is being studied in another project from the University Coal Research Program. The catalyst should be studied experimentally to determine what sulfur sources can be used (all studies to date used H<sub>2</sub>S) and what their critical concentrations are. For coal conversion processes, there will likely be a source of sulfur in the original coal, so the need for sulfur might not pose a significant problem. The performance of these catalysts should also be examined at higher temperatures to determine the range of operability.

## Conclusions

This investigation has demonstrated that the inhibition of water-gas shift activity by product CO<sub>2</sub> causes a very significant decrease in membrane reactor performance. The microkinetic model of the ferrochrome-catalyzed reaction suggested that weakening of surface oxygen bonds would lessen this effect. As a consequence, it was shown that copper-promoted catalysts are more effective, with the optimum copper loading being of the order of 10 wt.%. More generally, the study has shown, through membrane reactor simulation, that the catalytic reaction process is more limiting than the permeation process. This suggests that development efforts should be directed at identification of better catalysts rather than better membranes. Further, it has been shown that elimination of the inhibition by carbon dioxide is a better catalyst design objective than increasing catalytic activity. In a membrane reactor, excess steam is not needed to push the equilibrium conversion, but this investigation has shown that it is still desirable in order to slow the adiabatic temperature rise. Finally, preliminary consideration of sulfided CoMo/Al<sub>2</sub>O<sub>3</sub> catalysts suggests that they may be very good candidates for use in water-gas shift membrane reactors. They are not inhibited by carbon dioxide, but they do require lower temperatures and a continuous supply of sulfur. The critical question is whether a sulfur level can be established such that the catalysts remain active without poisoning the membrane material. This question has been left for future study.

## References

1. Bohlbro, H., *An Investigation on the Conversion of Carbon Monoxide with Water Vapour over Iron Oxide Based Catalysts*. 1969, Gjellerup, Copenhagen: Haldor Topsøe. 196.
2. Rase, H.F., *Chemical Reactor Design for Process Plants*. Vol. Two. 1977, New York: John Wiley. 242.
3. Lund, C.R.F., J.J. Schorfheide, and J.A. Dumesic, *Magnetite Surface Area Titration Using Nitric Oxide*. *J. Catal*, 1979. **57**: p. 105.
4. Dumesic, J.A., et al., *The Microkinetics of Heterogeneous Catalysis*. 1993, Washington, DC: American Chemical Society.
5. *NIST Standard Reference Database Number 69*. 2001.
6. *Athena Visual Workbench*. 1997, Stewart and Associates, Inc.
7. Shu, J., et al., *Catalytic Palladium-based Membrane Reactors: A Review*. *Can. J. Chem. Eng.*, 1991. **69**: p. 1036-1059.
8. Borekov, G.K., T.M. Yur'eva, and A.S. Sergeeva, *Mechanism of the Conversion of Carbon Monoxide on an Iron-Chromium Catalyst*. *Kinet. Catal.*, 1970. **11**(6): p. 1230-1232.
9. Kaneko, Y. and S. Oki, *J. Res. Inst. Catalysis, Hokkaido Univ.*, 1965. **13**: p. 55.
10. Kaneko, Y. and S. Oki, *J. Res. Inst. Catalysis, Hokkaido Univ.*, 1967. **15**: p. 185.
11. Mezaki, R. and S. Oki, *Locus of the Change in the Rate-Determining Step*. *J. Catal.*, 1973. **30**(3): p. 488-489.
12. Oki, S. and Y. Kaneko. in *ACS Conference*. 1979. Hawaii.
13. Oki, S. and R. Mezaki, *Identification of Rate-Controlling Steps for the Water-Gas Shift Reaction over an Iron Oxide Catalyst*. *J. Phys. Chem.*, 1973. **77**(4): p. 447-452.
14. Oki, S. and R. Mezaki, *Mechanistic Structure of the Water-Gas Shift Reaction in the Vicinity of Chemical Equilibrium*. *J. Phys. Chem.*, 1973. **77**(13): p. 1601-1605.
15. Oki, S. and R. Mezaki, *J. Catal.*, 1973. **30**: p. 488.
16. Shchbrya, G.G., N.M. Morozov, and M.I. Temkin, *The Kinetics and Mechanism of the Catalytic Reaction between Carbon Monoxide and Steam I. Reaction on Iron-Chromium Catalyst*. *Kinet. Catal.*, 1965. **6**(6): p. 955-965.
17. Hu, Y., et al., *Reactive behaviors of iron-based shift catalyst promoted by ceria*. *Chem. Eng. J.*, 2000. **78**: p. 147-152.
18. Kappen, P., J.-D. Grunwaldt, and B.S. Clausen, *The State of Cu Promoter Atoms in High-Temperature Shift Catalysts--An in Situ Fluorescence XAFS Study*. *Journal of catalysis*, 2001. **198**(1): p. 56.
19. Armor, J.N., *Catalysis with Permselective Inorganic Membranes*. *Appl. Catal.*, 1989. **49**: p. 1-25.
20. Lund, C.R.F., *Effect of Adding Co to MoS<sub>2</sub>/Al<sub>2</sub>O<sub>3</sub> upon the Kinetics of the Water-Gas Shift*. *Ind. Eng. Chem. Res.*, 1996. **35**(9): p. 3067-3073.
21. Lund, C.R.F., *Microkinetics of Water-Gas Shift over Sulfided Mo/Al<sub>2</sub>O<sub>3</sub> Catalysts*. *Ind. Eng. Chem. Res.*, 1996. **35**(8): p. 2531-2538.
22. Way, J.D. and R.L. McCormick. *Palladium/Copper Alloy Composite Membranes for High Temperature Hydrogen Separation From Coal-Derived Gas Streams*. in *University Coal Research Contractors Review Conference*. 2001. Pittsburgh, PA: NETL/DOE.

## Bibliography

### Publications Based upon this Project

“Assessing High-Temperature Water-Gas Shift Membrane Reactors.” C. R. F. Lund, *Ind. Eng. Chem. Res.*, **submitted** (2002).

“A Microkinetic Model for High Temperature Water-Gas Shift Emphasizing Operation at Membrane Reactor Conditions,” D. Ma, M. Zhang and C. R. F. Lund, *J. Catal.* **submitted** (2002).

“The Effects of Ce and Cu as Promoters for High Temperature Water-Gas Shift at Membrane Reactor Conditions,” M. Zhang and C. R. F. Lund, **in preparation** (2002).

### Presentations Based upon this Project

“Water Gas Shift at Membrane Reactor Conditions,” (poster) University Coal Research Contractors Review Meeting, Pittsburgh, PA, June 6-7, 2000.

“Water Gas Shift Kinetics under Membrane Reactor Conditions,” D. Ma and C. R. F. Lund, AIChE Annual Meeting, Los Angeles, CA, November 2000.

“Microkinetic Models for Water-Gas Shift at Membrane Reactor Conditions,” Chemical Engineering Department Seminar, Tufts University, March 26, 2001.

“Water-Gas Shift at Membrane Reactor Conditions,” University Coal Contractors Review Meeting, Pittsburgh, PA, June 5, 2001. Co-author: Z. Mang.

“Water-Gas Shift over Promoted Iron Oxide,” AIChE Annual Meeting, Reno, NV, November 2001. Co-author: Z. Mang.

“Water Gas Shift Kinetics at Membrane Reactor Conditions,” (poster) University Coal Contractors Review Meeting, Pittsburgh, PA, June 4, 2002.

“Water-Gas Shift Kinetics over Modified Iron Oxide Catalysts at Membrane Reactor Conditions,” Pittsburgh-Cleveland Catalysis Society Meeting, Monroeville, PA, May 10, 2002. Co-author: M. Zhang (speaker).

“High Temperature Water-Gas Shift at Membrane Reactor Conditions,” to be presented at the AIChE Annual Meeting, Indianapolis, IN, November 2002. Co-author: M. Zhang.

## Tables

Table 1. BET Surface Areas of Fresh and Used Catalysts.

BET Area (m <sup>2</sup> g <sup>-1</sup> )	Before Reaction	After Reaction
Fe <sub>3</sub> O <sub>4</sub>	37	15
FeCr	40	38
0.1% Cu/FeCr	34	32
1% Cu/FeCr	27	28
5% Cu/FeCr	26	24
10% Cu/FeCr	17	20
20% Cu/FeCr	15	17
CuO	<1	

Table 2. Parameters for the Six-Step Microkinetic Model.

Surface Species	S <sup>0</sup> (688K)* (J mol <sup>-1</sup> K <sup>-1</sup> )	-ΔH <sub>gas→surf</sub> (688K) (kJ mol <sup>-1</sup> )
O*	1.821E+01	6.01E+02
CO <sub>3</sub> * <sub>2</sub>	8.472E+01	7.48E+02
CO <sub>3</sub> *	9.472E+01	5.98E+02
H <sub>2</sub> O*	5.586E+01	1.07E+02
HO*	4.698E+01	4.13E+02
Reaction	k <sub>0</sub> * (s <sup>-1</sup> )	E (kJ mol <sup>-1</sup> )
CO + 2 O* ⇌ CO <sub>3</sub> * <sub>2</sub>	1.00E+06	0.00
CO <sub>3</sub> * <sub>2</sub> ⇌ CO <sub>3</sub> * + *	1.00E+13	150.03
CO <sub>3</sub> * ⇌ CO <sub>2</sub> + O*	1.00E+13	0.00
H <sub>2</sub> O + * ⇌ H <sub>2</sub> O*	1.00E+06	22.43
H <sub>2</sub> O* + O* ⇌ 2 HO*	1.00E+13	0.00
2 HO* ⇌ 2 O* + H <sub>2</sub>	1.00E+13	51.08

\* Fixed estimates not used as fitting parameters

Table 3. Parameters for the Two-Step Microkinetic Model.

Parameter	Adjusted or Fixed	Resulting Value
$-\Delta H_{O_{gas} \rightarrow O^*}^0$	Adjusted	602 kJ mol <sup>-1</sup>
$S_{O^*}^0$	Fixed	18.2 J mol <sup>-1</sup> K <sup>-1</sup>
$k_2^0$	Fixed	10 <sup>6</sup> atm <sup>-1</sup> s <sup>-1</sup>
$k_3^0$	Fixed	10 <sup>6</sup> atm <sup>-1</sup> s <sup>-1</sup>
$E_2$	Adjusted	72.5 kJ mol <sup>-1</sup>
$E_3$	Adjusted	27.5 kJ mol <sup>-1</sup>

Figures

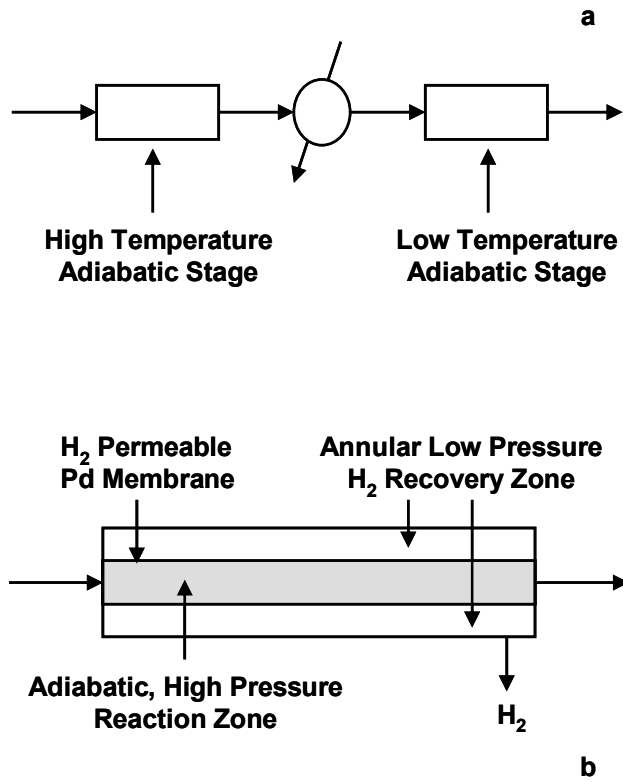


Figure 1. Schematic representation of (a) a conventional WGS reactor system, and (b) a WGS membrane reactor.

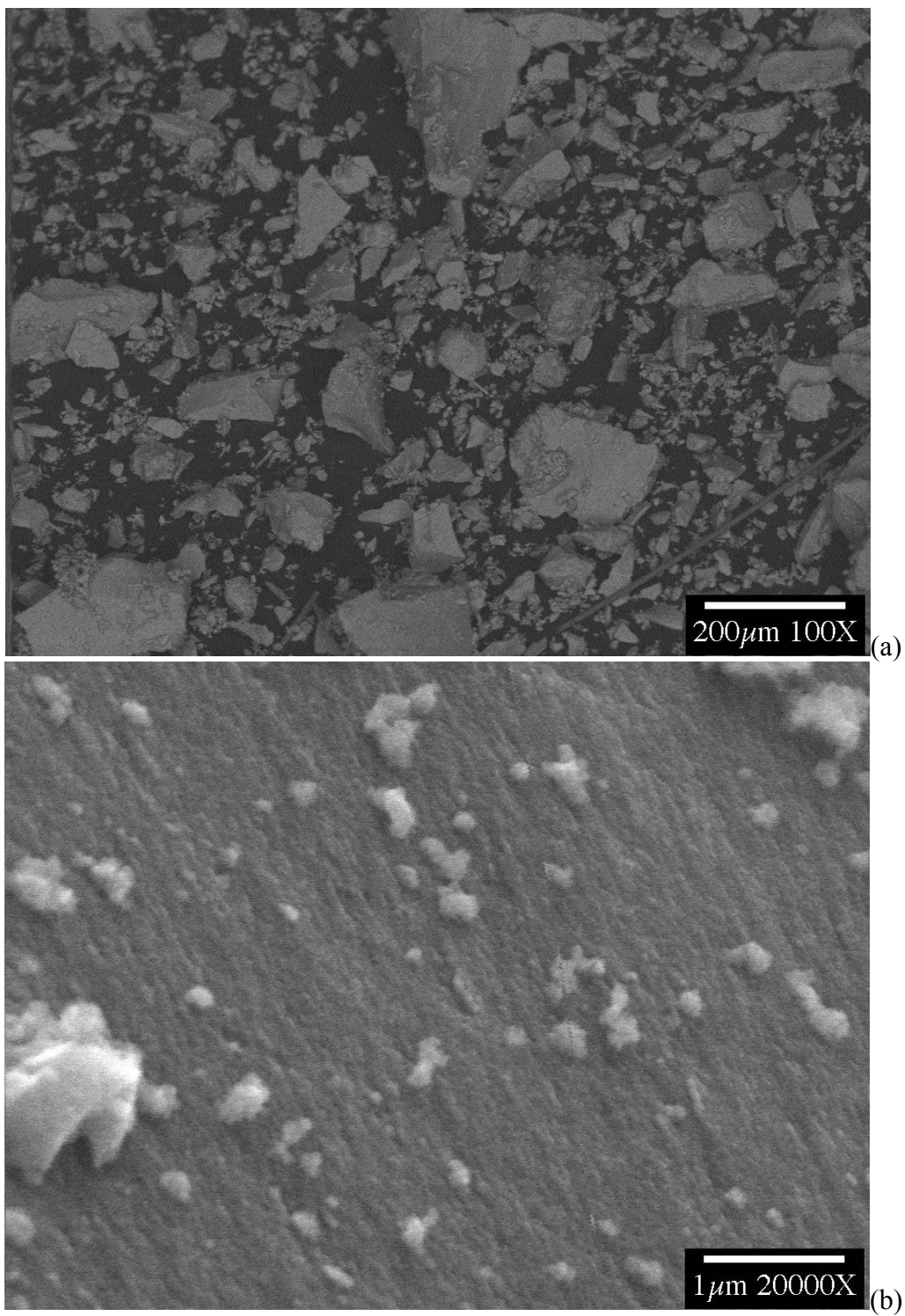


Figure 2. Low (a) and high (b) magnification SEM images of the FeCr catalyst from which Cu-promoted catalysts were prepared.

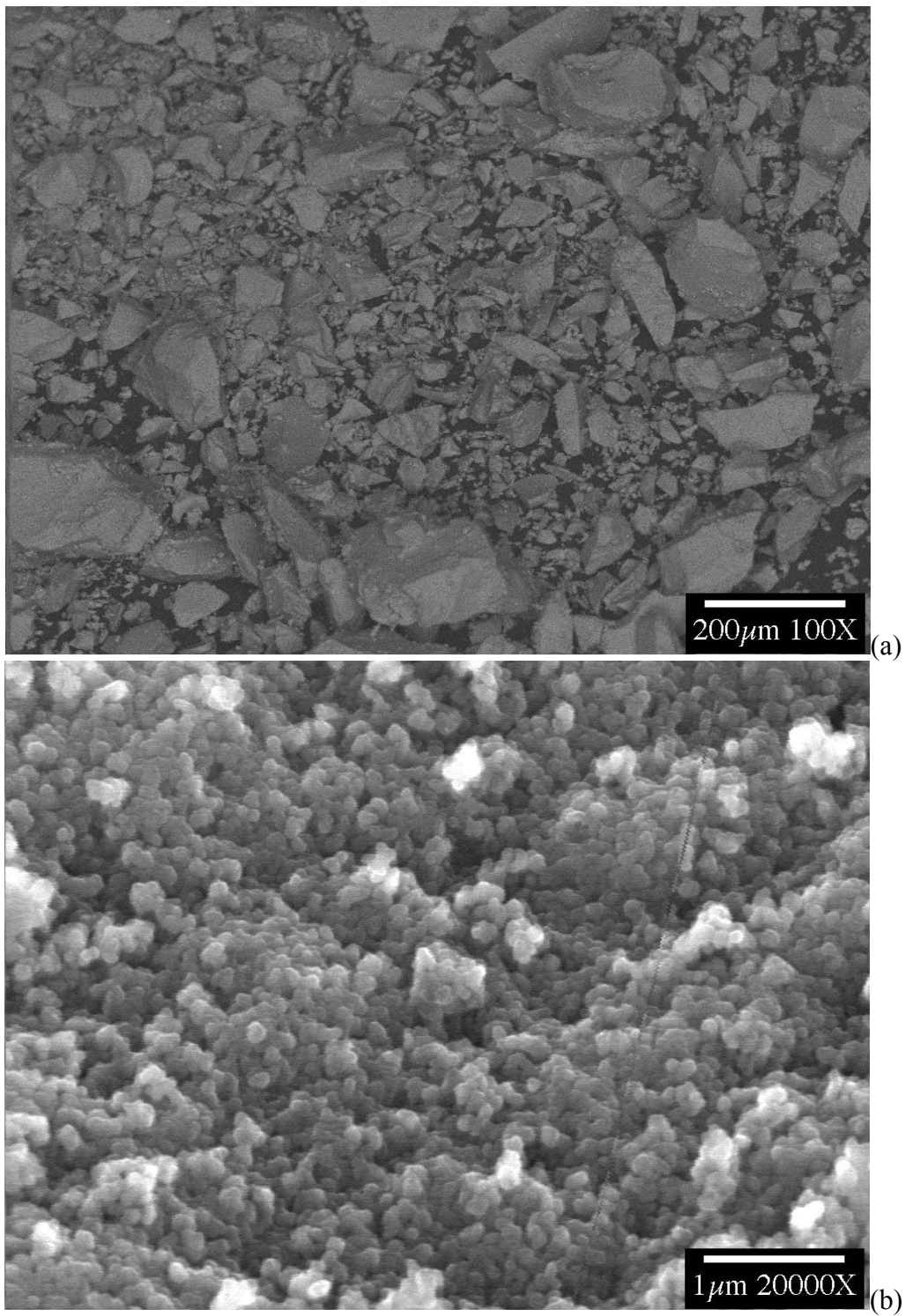


Figure 3. Low (a) and high (b) magnification SEM images of the FeCr catalyst promoted with 1 wt.% Cu.

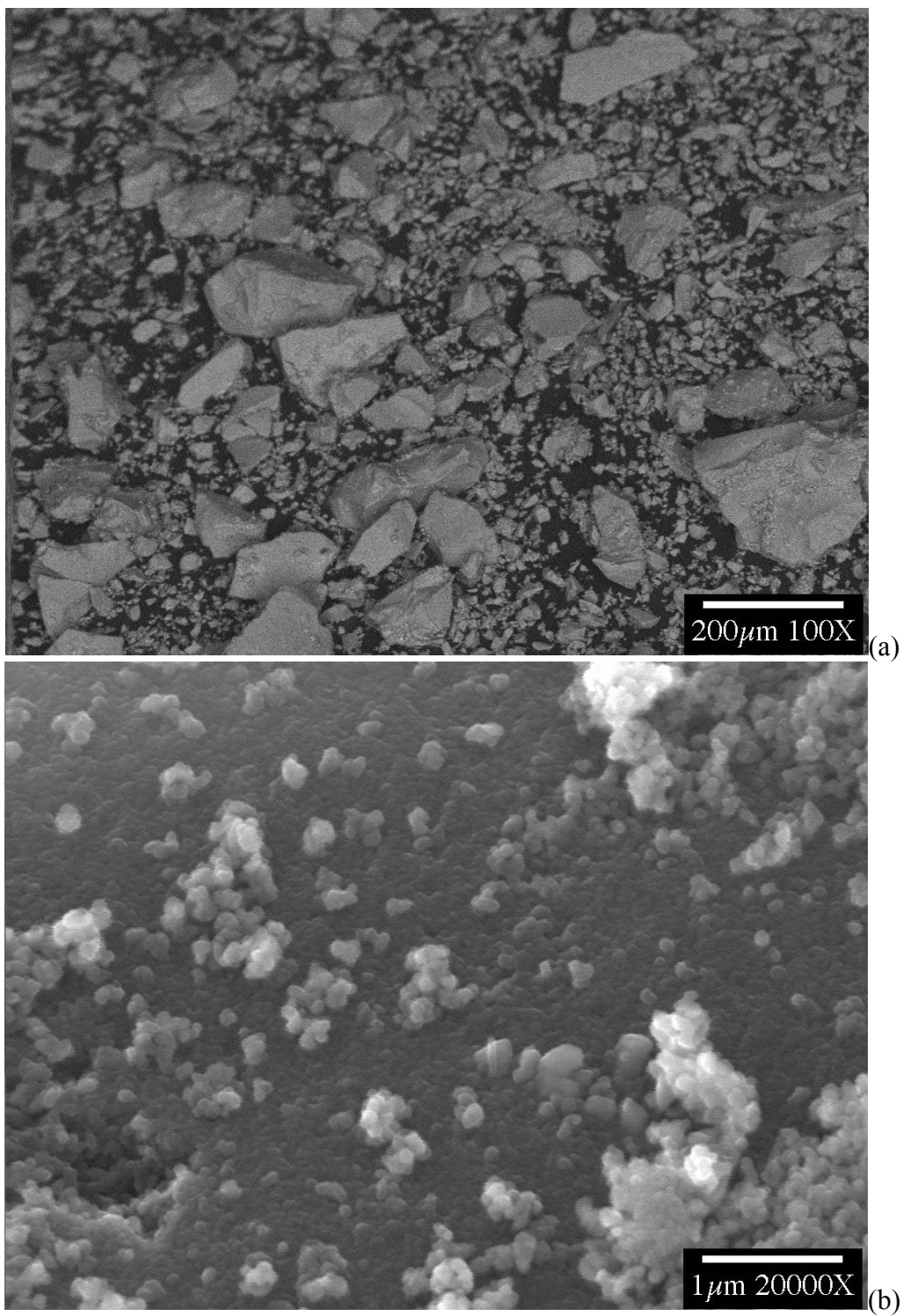


Figure 4. Low (a) and high (b) magnification SEM images of the FeCr catalyst promoted with 5 wt.% Cu.

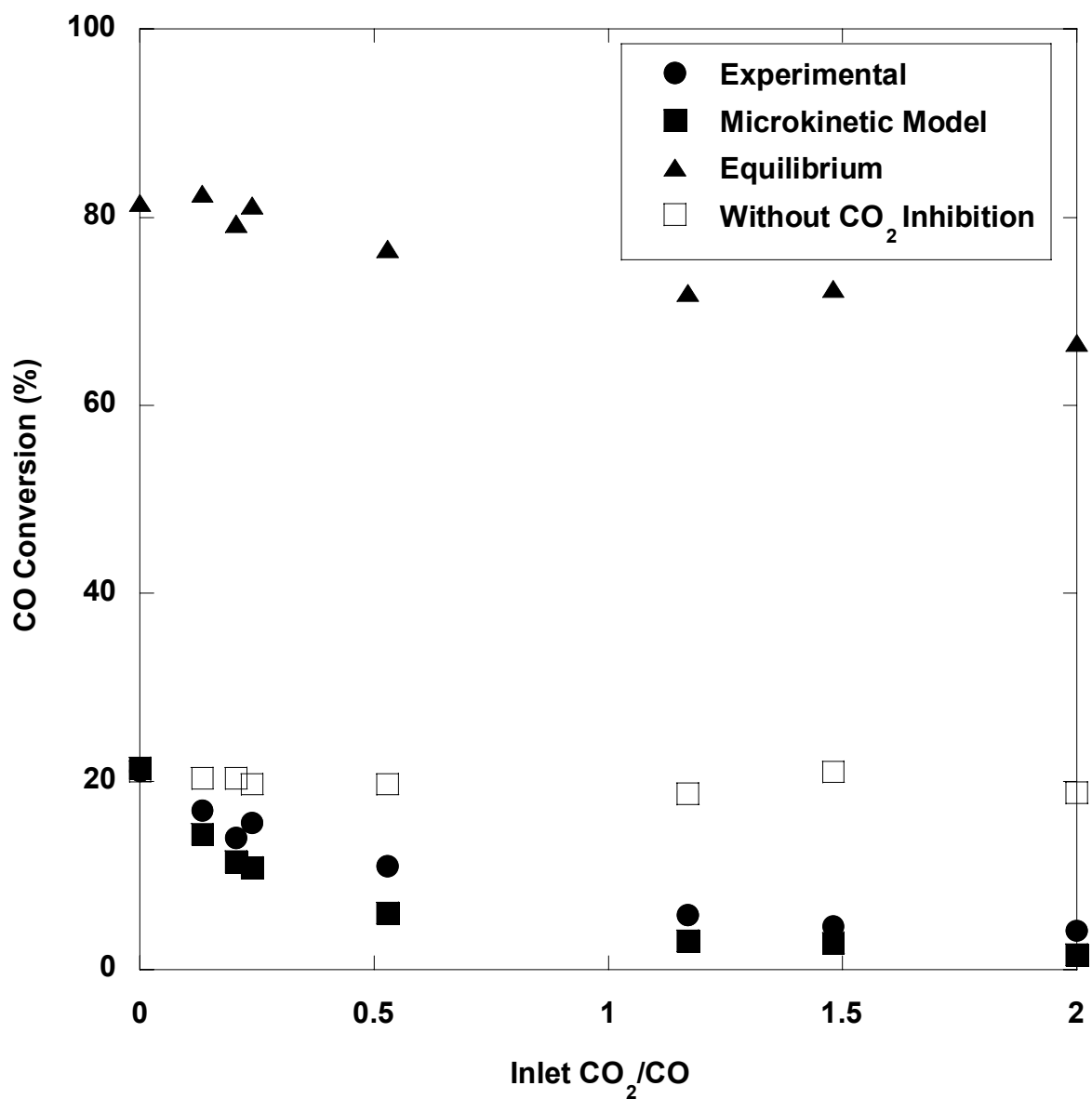


Figure 5. With the overall reaction far from thermodynamic equilibrium (filled triangles), inhibition of WGS catalyst activity by CO<sub>2</sub> is evident in Bohlbro's data (filled circles) and is captured by the two-step microkinetic model (filled squares). The unfilled squares show the behavior of a hypothetical catalyst where the inhibition by CO<sub>2</sub> has been mathematically eliminated as described in the text.

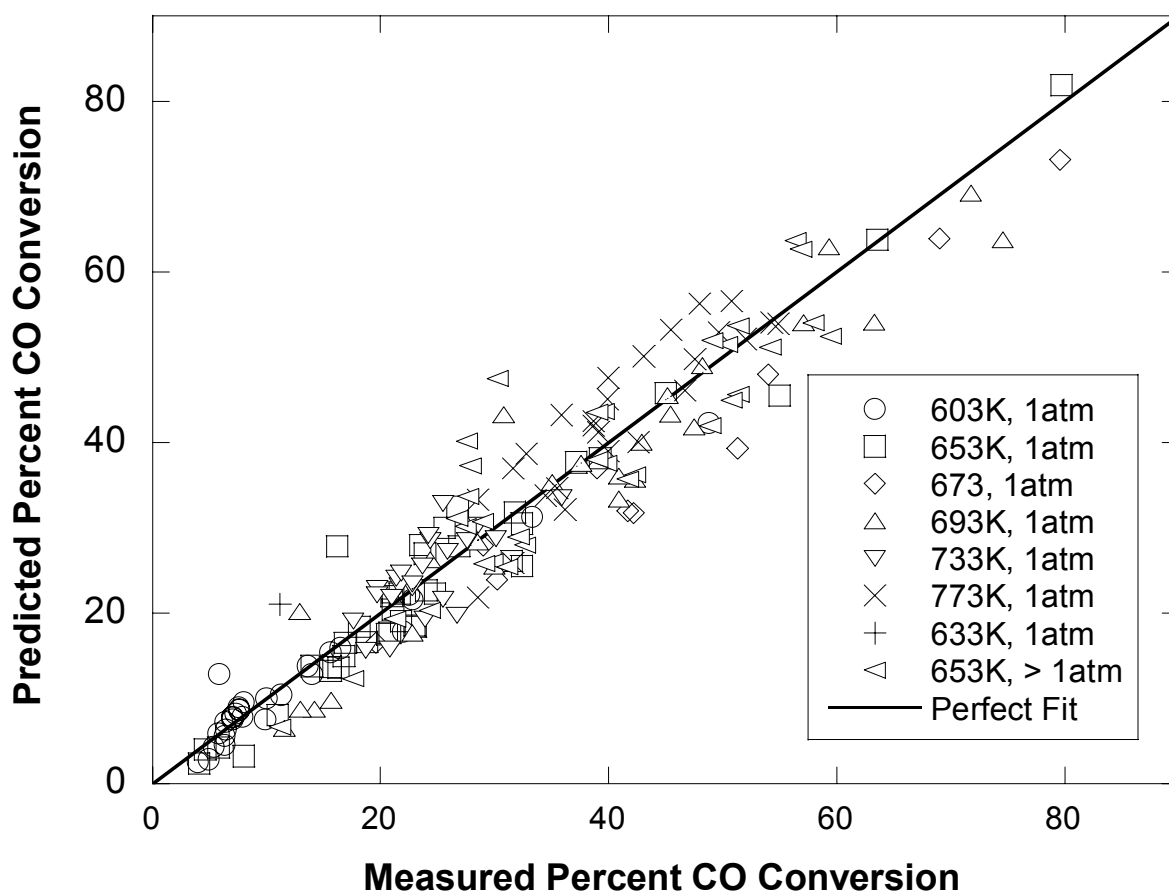


Figure 6. Carbon monoxide conversion predicted by the six step microkinetic mode compared to that measured experimentally by Bohlbro. Bohlbro's data have been grouped into sets with a common temperature and pressure.

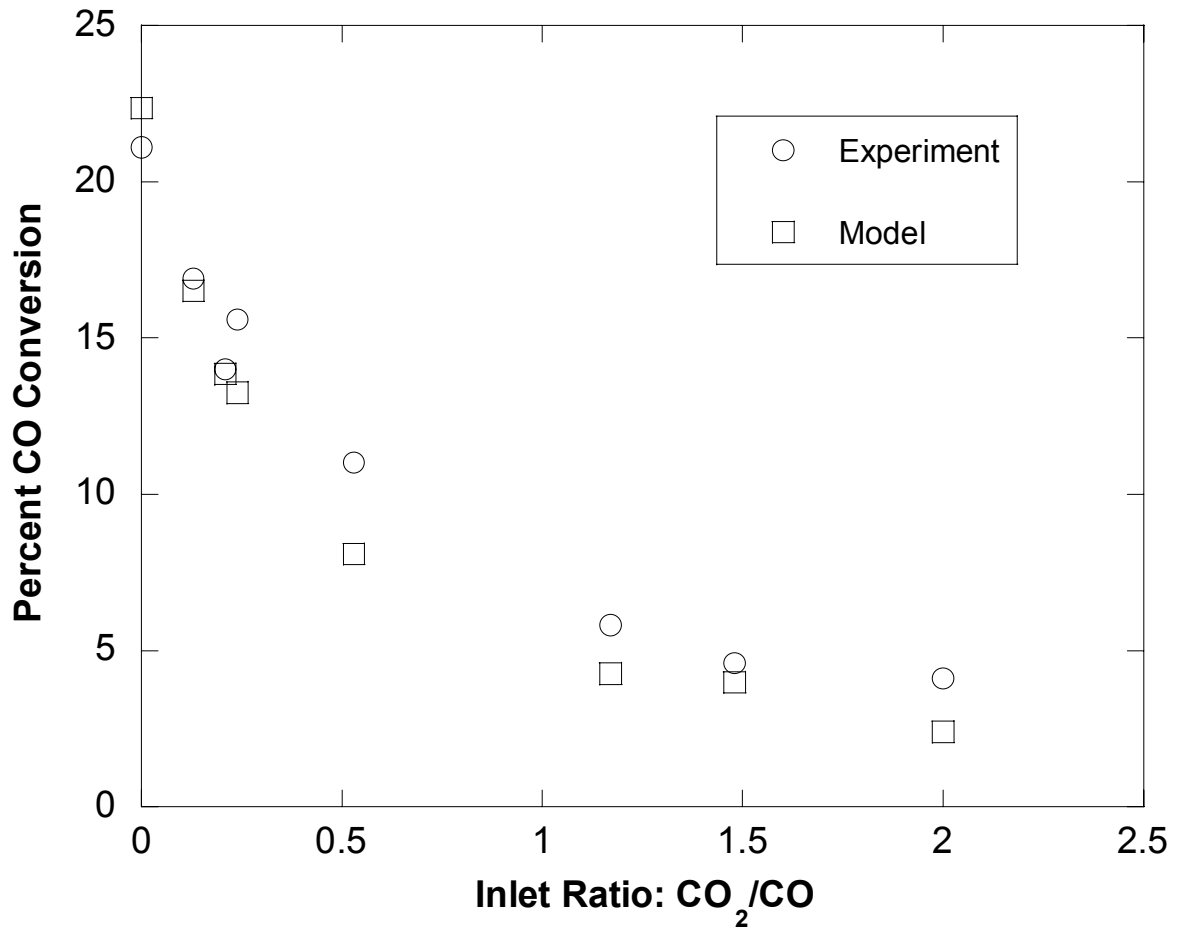


Figure 7. Comparison of the six step model predictions to experimentally measured CO conversions in a series of experiments at 653 K and 1 atm wherein Bohlbro varied the inlet CO<sub>2</sub> and N<sub>2</sub> partial pressures holding all other settings constant.

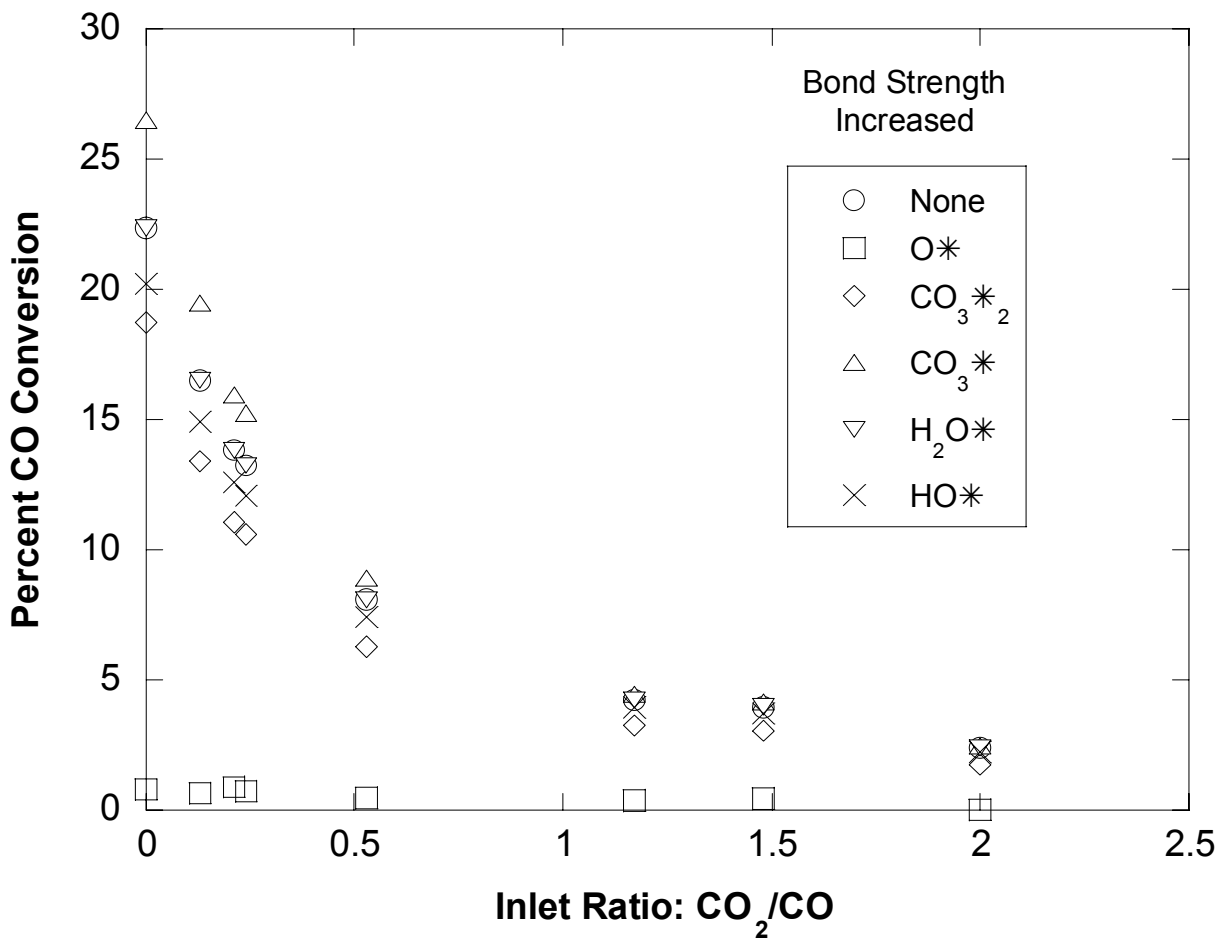


Figure 8. Simulated CO conversions for a set of “virtual” catalysts with one bond strength increased by 2% (1% in the case of HO\*) from the values given in Table 1; the simulated experiments correspond to those in Figure 7.

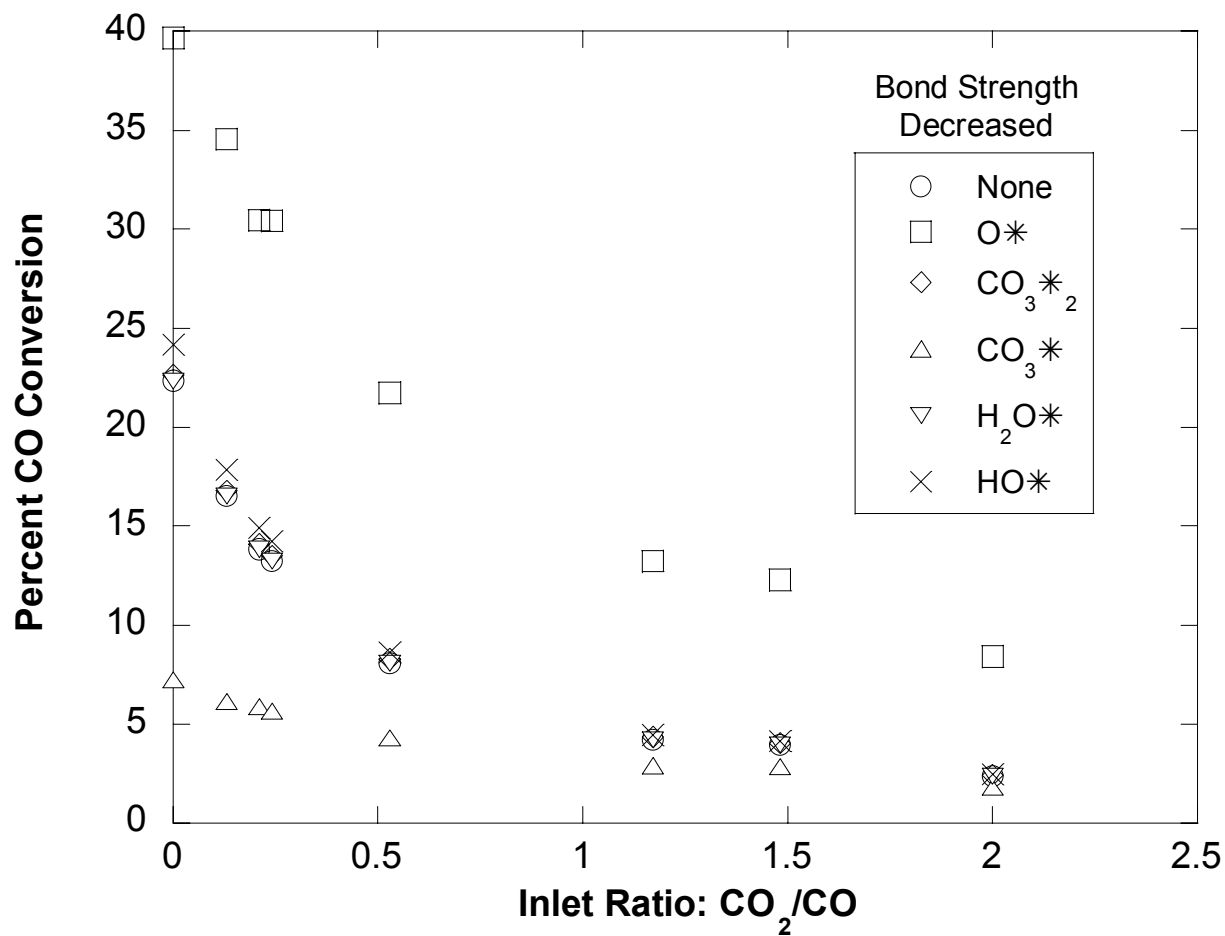


Figure 9. Simulated CO conversions for a set of “virtual” catalysts with one bond strength decreased by 2% from the values given in Table 1; the simulated experiments correspond to those in Figure 7.

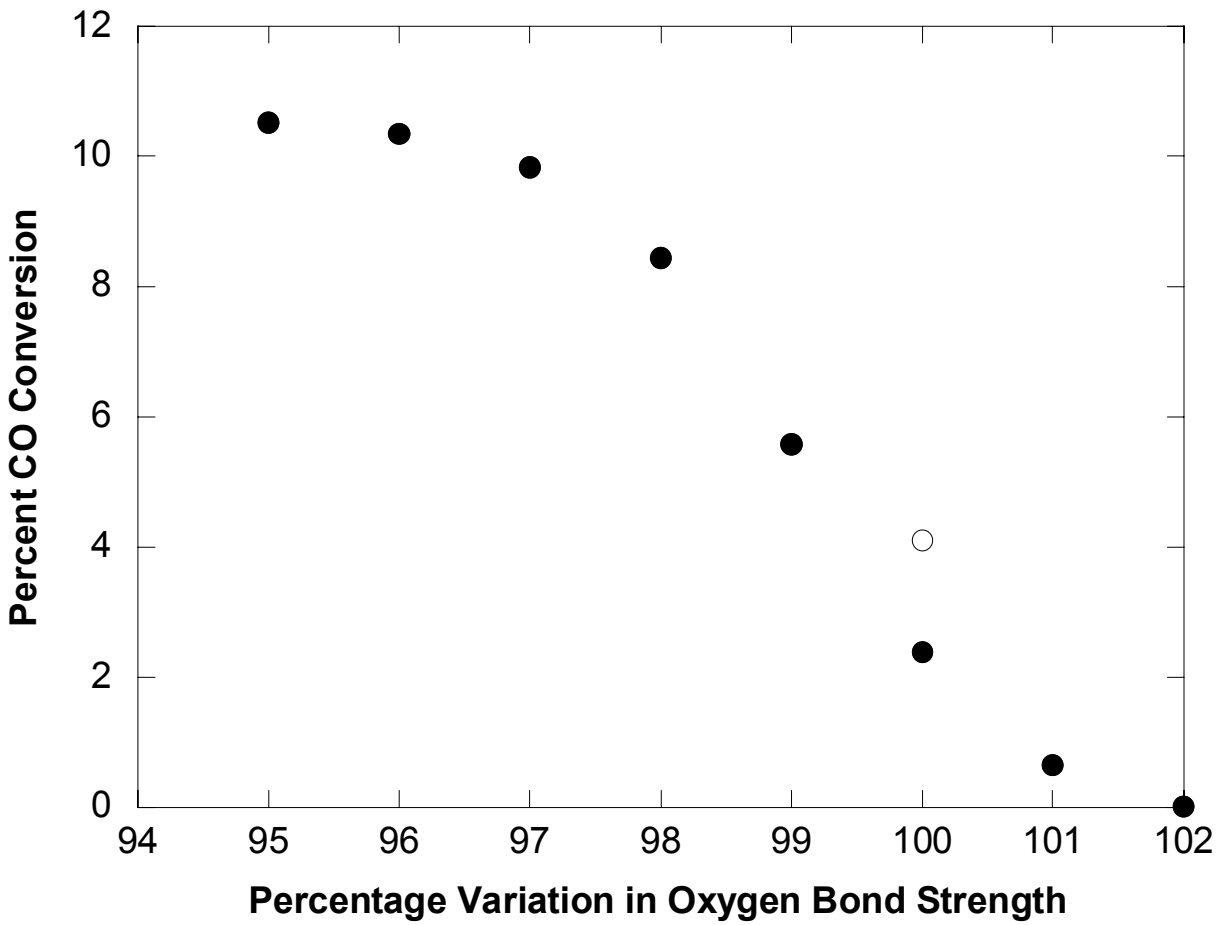


Figure 10. Simulated CO conversion as the O\* bond strength is varied from the value in Table 3; conditions correspond to the experiment in Figure 7 with an inlet CO<sub>2</sub>/CO ratio of 2.0.

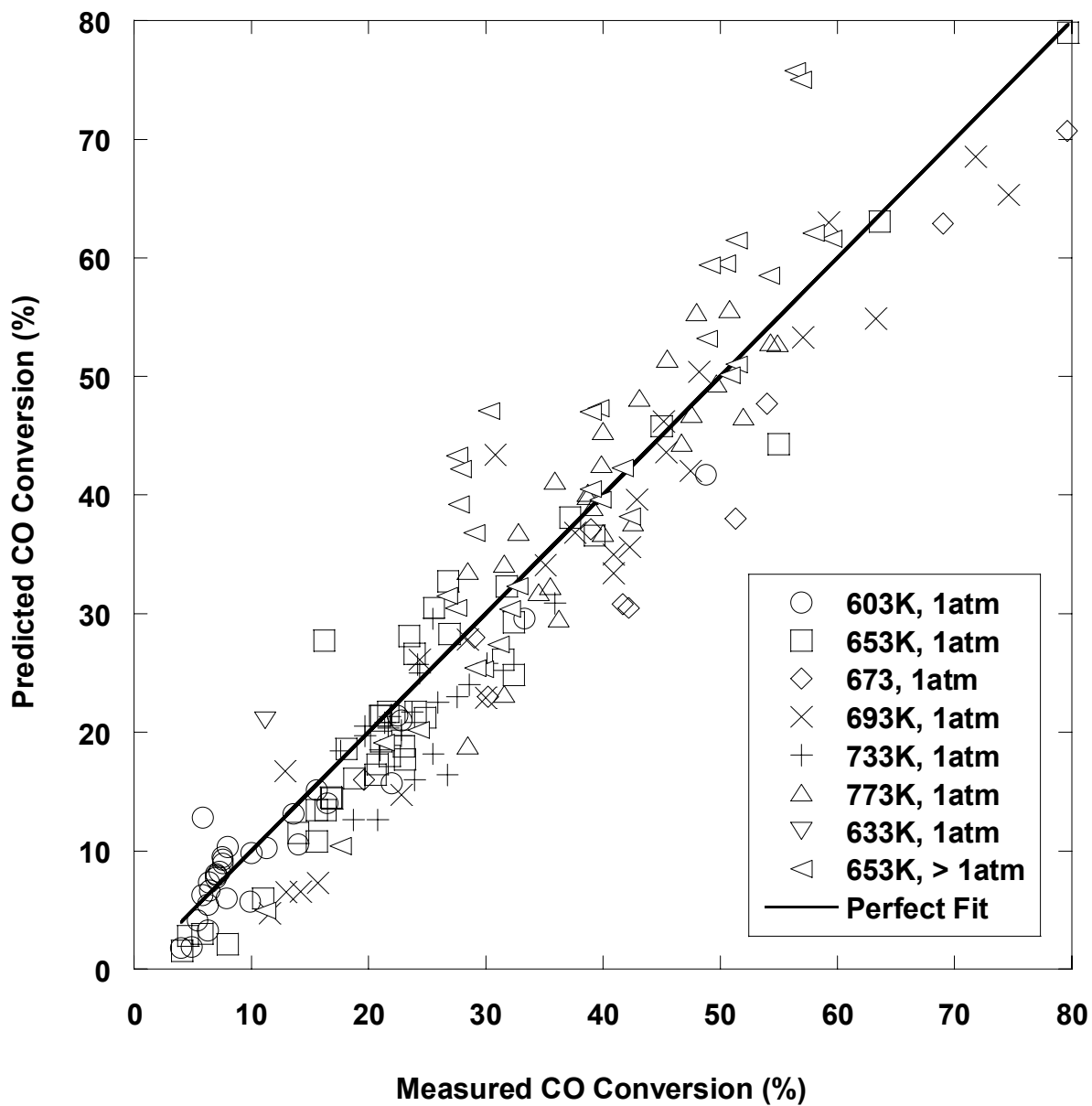


Figure 11. Carbon monoxide conversion predicted by the two step microkinetic mode compared to that measured experimentally by Bohlbro. Bohlbro's data have been grouped into sets with a common temperature and pressure.

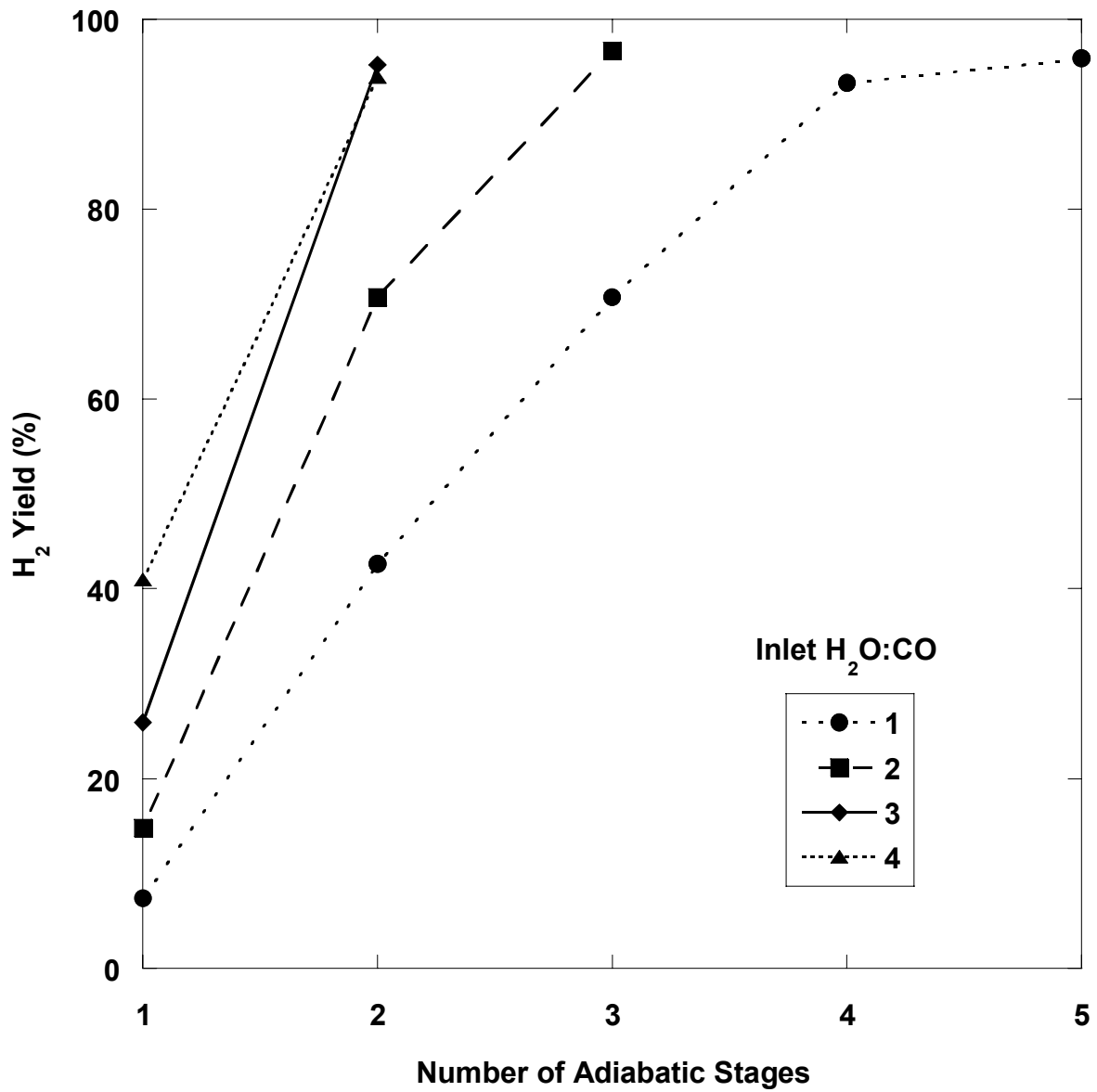


Figure 12. Effect of inlet steam to carbon monoxide ratio on the hydrogen yield and number of adiabatic stages.

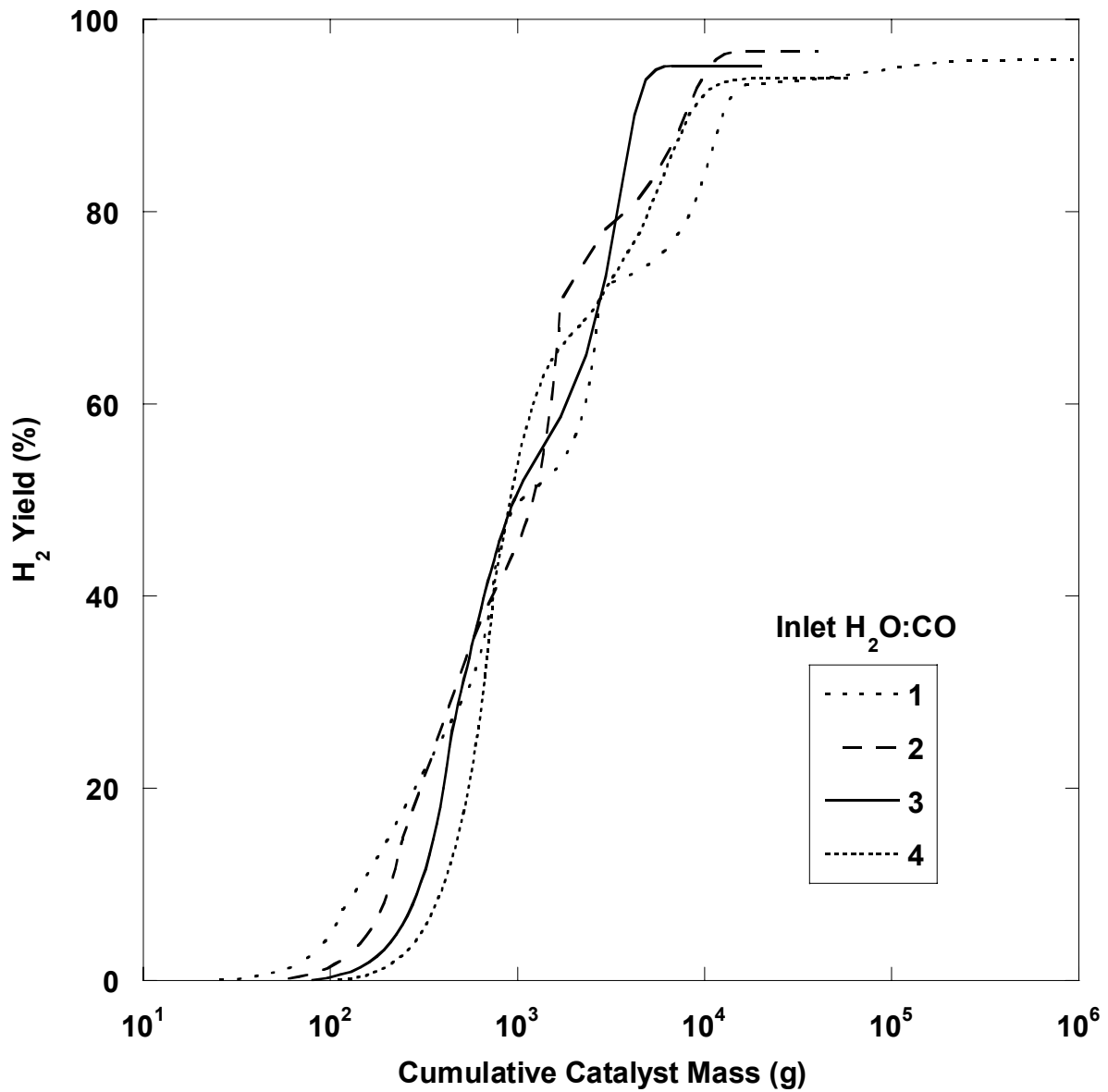


Figure 13. Hydrogen yield as a function of catalyst volume for staged adiabatic membrane reactors with varying inlet steam to carbon monoxide ratios.

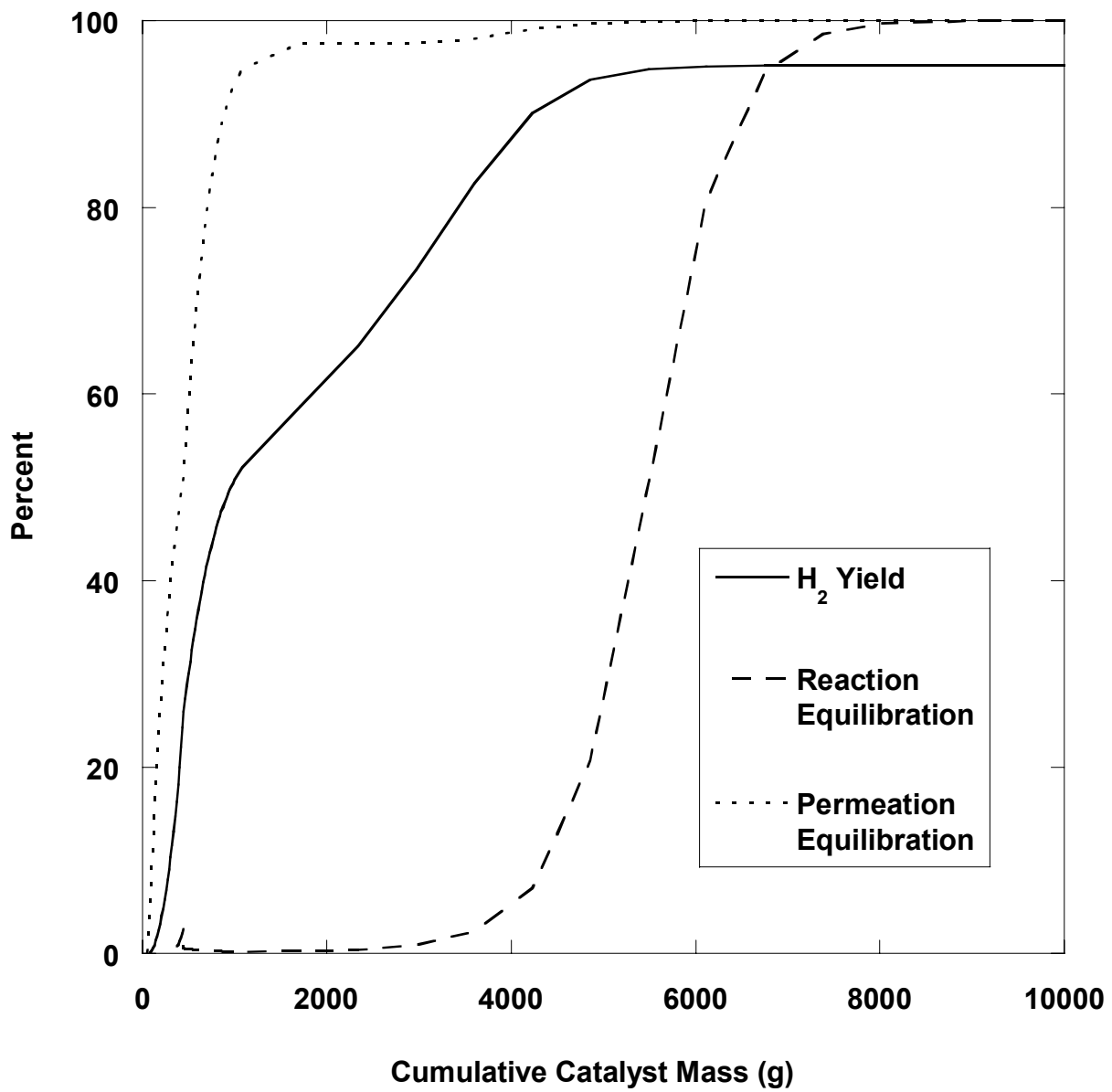


Figure 14. Variation in the percent of reaction equilibration and the percent of permeation equilibration along the length of an adiabatic staged membrane reactor.

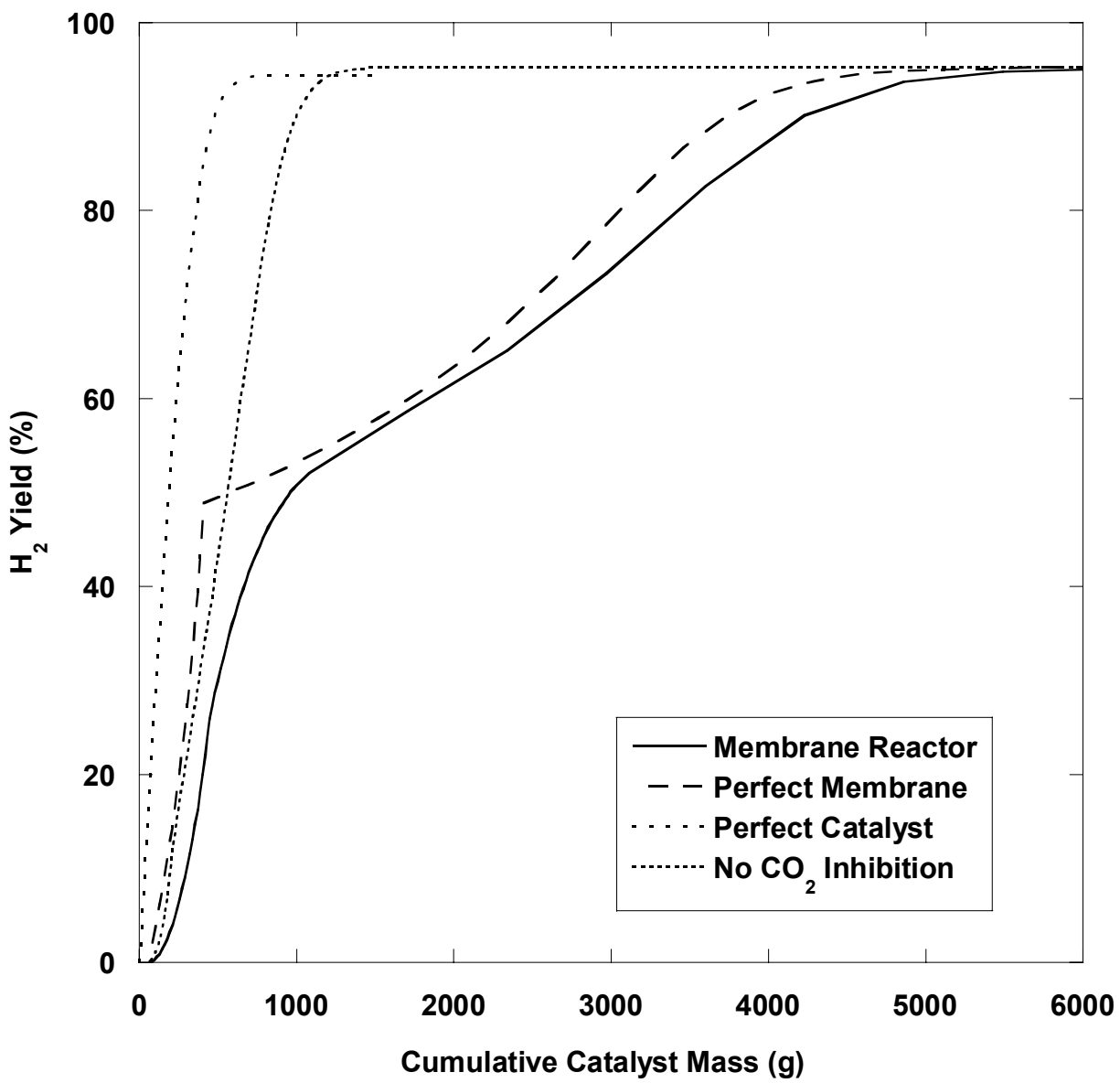


Figure 15. Comparison of the simulated membrane reactor yield to idealized membrane reactors where either the membrane is perfect, the catalyst is perfect or the catalyst does not suffer from CO<sub>2</sub> inhibition.

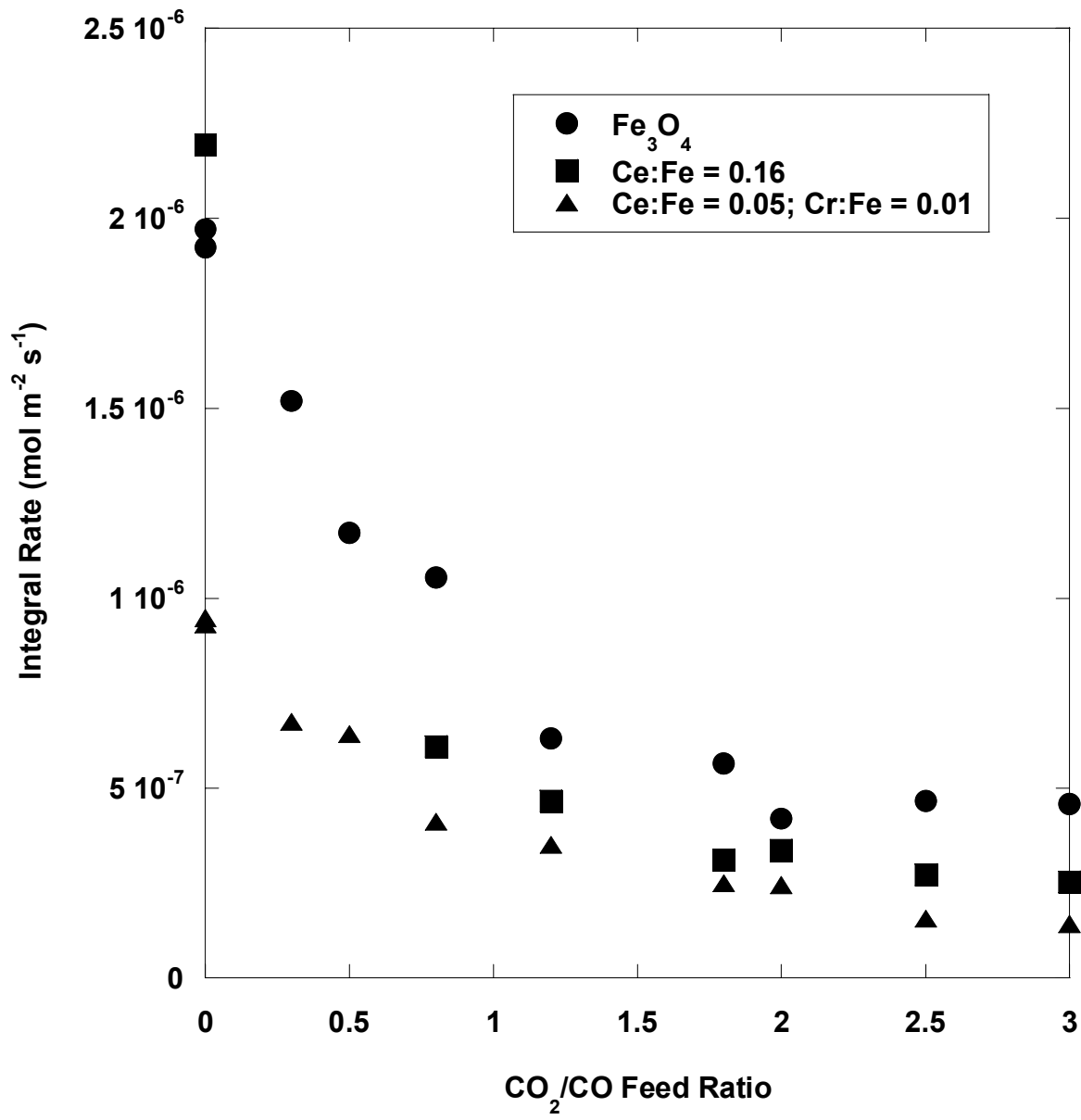


Figure 16. Effect of Ce promoters on the activity of iron oxide WGS catalysts.

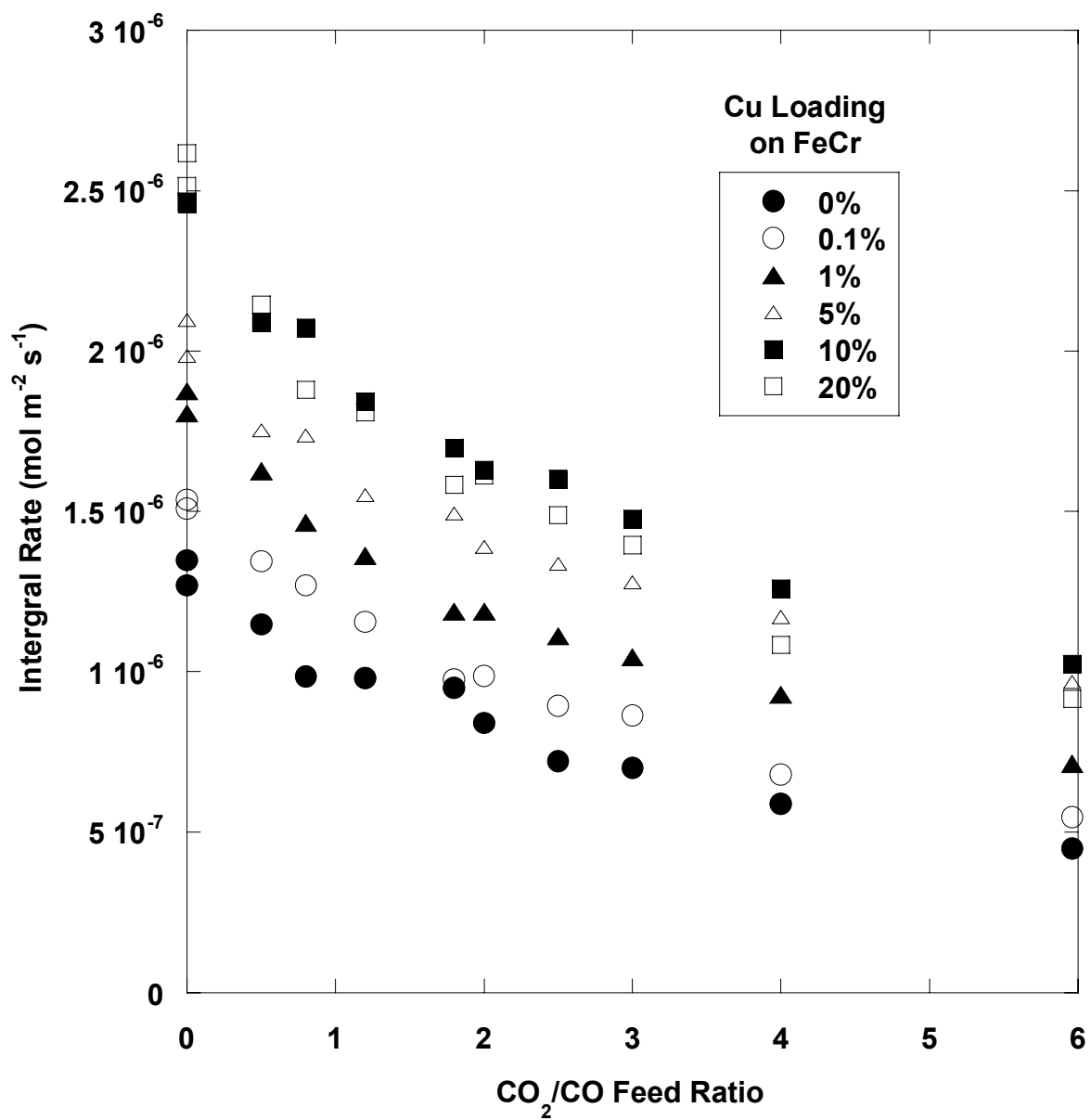


Figure 17. Effect of Cu promoter loading upon catalytic activity at membrane reactor conditions.

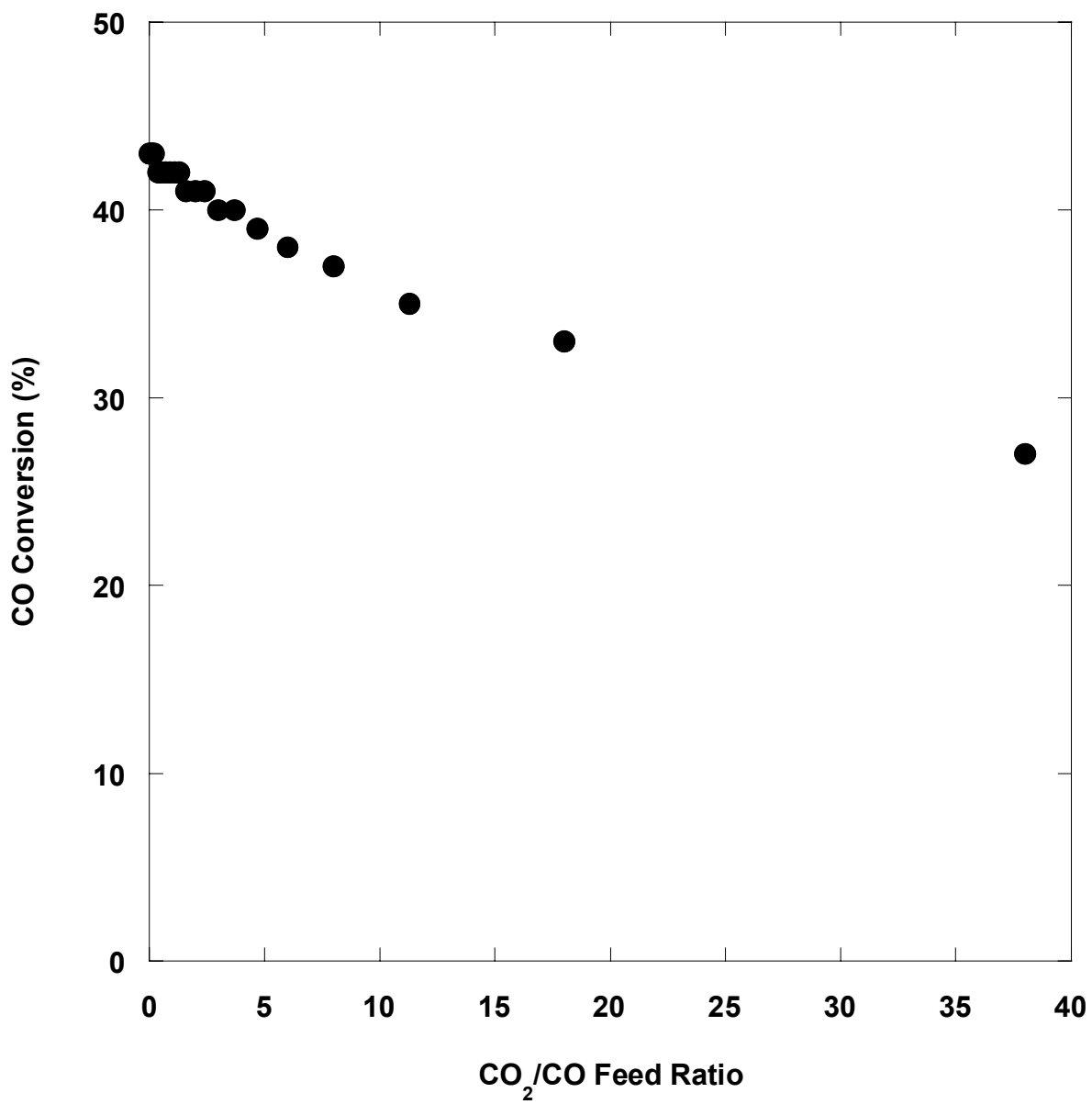


Figure 18. Effect of CO<sub>2</sub> upon the water-gas shift activity of sulfided CoMo/Al<sub>2</sub>O<sub>3</sub>.